

A Barotropic Model of the Angular Momentum–Conserving Potential Vorticity Staircase in Spherical Geometry

TIMOTHY J. DUNKERTON AND RICHARD K. SCOTT

Northwest Research Associates, Bellevue, Washington

(Manuscript received 23 June 2006, in final form 21 February 2007)

ABSTRACT

An idealized analytical model of the barotropic potential vorticity (PV) staircase is constructed, constrained by global conservation of absolute angular momentum, perfect homogenization of PV in mixing zones between (prograde) westerly jets, and the requirement of barotropic stability. An imposed functional relationship is also assumed between jet speed and latitudinal separation using a multiple of the “dynamical Rossby wave” Rhines scale inferred from the strength of westerly jets. The relative simplicity of the barotropic system provides a simple relation between absolute angular momentum and PV (or absolute vorticity). A family of solutions comprising an arbitrary number of jets is constructed and is used to illustrate the restriction of jet spacing and strength imposed by the constraints of global conservation of angular momentum and barotropic stability. Asymptotic analysis of the theoretical solution indicates a limiting ratio of jet spacing to the dynamical Rhines scale equal to the square root of 6, meaning that westerly jets are spaced farther apart than predicted by the dynamical Rhines scale. It is inferred that an alternative “geometrical” Rhines scale for jet spacing can be obtained from conservation of absolute angular momentum on the sphere if the strength of zonal jets is known from other considerations. Numerical simulations of the full (nonaxisymmetric) equations reveal a pattern of zonal jet evolution that is consistent with our construction of ideal PV staircases in spherical geometry (which can be considered as limiting cases), as well as with the asymptotic analysis of a geometrical Rhines scale. The evolution of the PV staircase originating from an upscale cascade of energy in the barotropic model is therefore seen to depend on conservation of energy (for the strength of jets) and conservation of absolute angular momentum (for the spacing and number of jets). Further analysis of the numerical results confirms a “Taylor identity” relating the flux of eddy potential vorticity to mean-flow acceleration. Eddy fluxes are responsible for the occasional transitions between mode number as well as for maintaining the sharp westerly jets against small-scale dissipation. Suggestions are made for extending the theoretical model to PV staircases that are asymmetric between hemispheres or with latitudinal variation of amplitude, as modeled in the shallow-water system.

1. Introduction

The concept of “geophysical turbulence” when applied to the large-scale circulation of planetary atmospheres must account for the emergence of coherent structures, most notably zonal jets of alternating sign that organize the turbulence into latitudinal bands. This result is consistent with the role of Rossby waves in arresting the upscale cascade of energy in barotropic or geostrophic turbulence (Rhines 1975; Williams 1978). Certain fundamental characteristics of turbulence, such

as disorder, similarity, and power-law behavior, are uncharacteristic of the zonal-mean zonal flow, which is ordered, coherent, and contributes to a steepened spectral slope with a distinct concentration of energy in the zonal component at low wavenumbers:

- 1) The mean zonal flow is *ordered* in the sense that (i) its temporal evolution from rest in a forced-dissipative system is monotonic, punctuated by occasional transitions of flow regime, and (ii) its maintenance in steady state (if the design of the numerical experiment allows such) is achieved by a balance of statistically stationary eddy fluxes and dissipative processes (typically some combination of hyperdiffusion at small scales and Rayleigh friction or hypodiffusion at large scales), both of which display a

Corresponding author address: Timothy J. Dunkerton, Northwest Research Associates, P.O. Box 3027, Bellevue, WA 98009.
E-mail: tim@nwra.com

consistent and predictable relationship to the jets themselves (Huang and Robinson 1998).

- 2) The mean zonal flow is *coherent* in the sense that it has a well-defined, quasi-periodic latitudinal structure (Danilov and Gurarie 2004) whose variation in latitude on the sphere, and relationship between jet strength and spacing, are in large measure reproducible and therefore predictable on theoretical grounds. Jet spacing is positively correlated with jet strength (Huang and Robinson 1998) or rate of energy injection (Maltrud and Vallis 1991; Scott and Polvani 2007). Simplicity of flow regimes is seen notwithstanding the well-known fact that the flow evolution in these very experiments (whether forced or freely decaying) is unpredictable in different realizations and may lead (from identical parameter settings but different initial conditions or random forcings) to flows of opposing symmetry: for example, in equatorial superrotation versus subrotation (Kitamura and Ishioka 2007).
- 3) As a coherent structure, the mean zonal flow causes the lower half of the wavenumber spectrum to depart significantly from predictions of isotropic quasi-2D turbulence with its “ -3 slope” downscale enstrophy cascade and “ $-5/3$ slope” upscale energy cascade. The zonal component instead exhibits a much steeper slope approaching -5 (Galperin et al. 2001), but it is questionable as to whether the concept of an energy spectrum is useful owing to the regular spatial structure of the zonal mean component (G. Vallis 2006, personal communication). Interestingly, if this component is notched out of the spectrum, the remaining nonzonal component displays an energy spectrum resembling quasi-2D turbulence (Huang et al. 2001; Danilov and Gurarie 2004). Geophysical turbulence therefore has a critical role to play in the evolution and maintenance of the coherent structures. To some extent this role can be anticipated by spectral thinking (Vallis and Maltrud 1993), but ultimately it becomes necessary to understand wave and turbulent transport *processes* in order to explain the evolution and maintenance of jets (Huang and Robinson 1998).

Between the wave and turbulent spectral regimes is the so-called *dynamical* Rhines scale, defined most simply as (i) the scale at which Rossby waves break and cease to exist, giving way to turbulence (proceeding to smaller spatial scales) or (ii) the scale at which the upscale turbulent transfer of energy is arrested by the excitation of Rossby waves (proceeding to larger spatial scales). An alternative definition of the Rhines scale, or *spectral* Rhines scale, was introduced by Maltrud and

Vallis (1991) in terms of the upscale transfer of energy. Their definition has the advantage that one can predict a transition scale based on knowledge of the rate of energy injection at small scales. As just noted, however, the emergence of coherent structures cannot be anticipated from spectral thinking alone. The role of Rossby waves and their associated eddies resulting, for example, from wave breaking or the excitation of smaller solitary waves and vortices, must be accounted for. This aspect of the problem involves wave–mean flow interaction, but having said this in no way guarantees that the evolution and maintenance of coherent structures is easy to understand. Based on the limited information currently available, we infer *three possible scenarios* for the organization of wave and turbulent transport by persistent zonal jets: 1) The first scenario is deduced from the consideration that (prograde) westerly jets cannot be the locus of a Rossby wave critical level; therefore, the jet latitude is a point of minimum parcel displacement and latitudinal stirring (Dunkerton and O’Sullivan 1996). The resulting “potential vorticity (PV) staircase” associated with a profile of westerly jets (McIntyre 1982; McIntyre and Palmer 1983, 1984; Peltier and Stuhne 2002) is then regarded as a natural outgrowth of the resting planetary profile of PV, which is an unstable equilibrium in the presence of Rossby waves and instabilities. The associated meridional profile of mean zonal wind organizes eddy momentum fluxes so as to maintain the staircase (Dunkerton 1991a; Randel and Held 1991; Del Sole 2001). 2) A second scenario also involves wave activity but recognizes that westerly jets may act as waveguides owing to their curvature (Simmons 1974), rather than directing wave activity to regions of weaker westerlies (Dickinson 1968). Steepened PV gradients ultimately become the locus of edge waves (Scott et al. 2004) when approaching the staircase limit. In a three-dimensional flow, edge waves propagate vertically on the jumps of the staircase and are evanescent on the steps in between. In flows with small-scale dissipation, wave fluxes may act locally to maintain westerly jets and their sharp meridional PV gradients. 3) A third scenario emphasizes the role of latitudinal shear in organizing small-scale eddy momentum fluxes in such a way as to maintain the jets (Huang and Robinson 1998). As eddies are rotated by shear, their meridional flux of zonal momentum is eventually altered to reinforce the shear. Whether this scenario involves a continuum of waves, or is simply the outcome of turbulence modified by persistent local shears, remains unclear. In the latter case there is no a priori distinction between (prograde) westerly and (retrograde) easterly jets; the locus and morphology of turbulent eddies evidently must depend on some other

process (most likely Rossby wave propagation) that excites or modulates the turbulence in the first place. Likewise, the effect of latitudinal shear on the continuum (the so-called Orr mechanism) does not differentiate between the sign of the shear, so in order to create or maintain a PV staircase this mechanism, too, must depend in some way on underlying asymmetries in wave propagation.

A better understanding of each of these scenarios (and possibly others) is needed for a comprehensive understanding of PV staircases. Particular attention should be given to eddy fluxes of PV that create and maintain the jets against dissipation. Do these fluxes act primarily (i) to maintain the (prograde) westerly jets in their cores, (ii) to maintain the (retrograde) easterly jets in between, or (iii) both? The answer to this question is likely a function of the scenario observed, as well as the dimensionality of the system. A multilayer system, for example, admits vertical wave propagation of quasi-stationary planetary waves that anchor easterly jets via heat fluxes while baroclinic eddies maintain the staircase via momentum fluxes (Lee 2005). All of our scenarios have a common characteristic that lateral eddy mixing is *inhomogeneous in latitude* and is *organized by the PV staircase* in such a way as to maintain it. The notion of inhomogeneous mixing in the context of Rossby wave–mean flow interaction appeared 25 yr ago in McIntyre’s (1982) review of sudden warmings and the related discussion by McIntyre and Palmer (1983) of a midlatitude “surf zone” bounded on both sides by sharp gradients¹ of PV and tracer: that is, the *circumpolar vortex edge* and (what later came to be known as) the *subtropical transport barrier*. Although the stratospheric flow is diabatically forced, actual gradients are much sharper than anticipated from diabatic effects alone (Butchart and Remsberg 1986). Clearly, large-scale planetary waves and specific flow features such as the Aleutian anticyclone are instrumental, if not essential, to the PV staircase of the terrestrial stratosphere and its extension to the terrestrial mesosphere (Dunkerton and Delisi 1985). This situation contrasts with the deep oceans of Earth and the visible atmospheres of gas giants (Jupiter, Saturn, etc.), where large-scale waves are less evident and (to the extent that we can observe them) the flows are dominated by smaller-scale eddies (Williams 1978; Galperin et al. 2004; Ingersoll et al. 2004) and, presumably, the transports associated with such eddies.

From the preceding discussion we infer that litera-

¹ Inhomogeneous mixing is also seen in the spontaneous development of a density staircase in freely decaying stratified turbulence (Ruddick et al. 1989; Holford and Linden 1999).

ture on the PV staircase has been motivated by a two-fold desire (i) to explain the banded structure of observed atmospheres in our solar system and terrestrial oceans, and (ii) to understand better the implications of Rossby waves and the Rhines scale for geophysical turbulence in rotating, stratified flows, whether on the β plane or sphere. The concept of the Rhines scale extends to spherical geometry, with certain complications arising from the latitudinal variation of β (Cho and Polvani 1996; Huang and Robinson 1998) and the tendency of shallow motions to be equatorially trapped (Theiss 2004; Scott and Polvani 2007). In one respect the sphere is a simpler system than the β plane because the latitudinal variations of β and deformation radius in effect lock the PV staircase to a fixed pattern that cannot drift in latitude (apart from occasional merger of jets). Going to the sphere we sacrifice the perfectly regular jet pattern of the β plane (Danilov and Gurarie 2004) but are able to glean useful information from the latitudinal variation of jet structure (Yoden and Yamada 1993; Huang and Robinson 1998; Scott and Polvani 2007) as emphasized in the discussion to follow. A local application of the β -plane model to the sphere was advocated recently by Theiss (2004) and Smith (2004).

As is clear from the title of our paper, another important aspect in the barotropic and shallow-water systems is the conservation of absolute angular momentum. Despite occasional recognition of the importance of this global invariant (Williams 1978; Yoden and Yamada 1993; Dritschel and McIntyre 2007) there has been surprisingly little discussion of the role of angular momentum conservation in building the PV staircase. This is in contrast to the repeated emphasis given to conservation of energy and the many factors that regulate the flux of energy and its accumulation or dissipation in various parts of the spectrum. Conservation of angular momentum has been a guiding principle in understanding nonlinear Hadley circulations in the terrestrial troposphere (Held and Hou 1980; Lindzen and Hou 1988; Plumb and Hou 1992) and stratosphere (Dunkerton 1989, 1991b; Tung and Kinnersley 2001) and on Mars (Schneider 1983). In a three-dimensional flow, overturning circulations are required to maintain gradient balance in the presence of thermal and mechanical forcings. Multijet flows are accompanied by multiple overturning circulations (James and Gray 1986).

The discussion to follow will make clear that PV staircases require consideration of the dual conservation of energy and angular momentum. Our conclusion is based on a mathematical analysis that takes into account the conservation laws, spherical geometry, and a requirement that the staircase be barotropically stable,

and is guided by recent numerical findings. Conservation of absolute angular momentum imposes a constraint on possible flows that may arise in geostrophic turbulence on the sphere, extending from the tropics to midlatitudes, or as far as the staircase extends. A scaling relation (in effect, law) will be derived relating the spacing of (prograde) westerly jets to their latitudinal spacing in terms of a “geometrical Rhines scale” whose definition is independent of the details of wave transport, PV mixing, and turbulence phenomenology. We merely require a PV staircase that (i) is completely homogenized within mixing zones located between (prograde) westerly jets and (ii) is barotropically stable. For simplicity and economy of presentation, discussion in sections 2 and 3 is limited to the barotropic case with hemispheric symmetry. Suggestions are offered in section 4 on how to extend the theory to asymmetric configurations and those with latitudinal variation of jet amplitude as arise in the shallow-water system. The theory is illustrated in section 3 using a barotropic version of the numerical model described by Scott and Polvani (2007).

2. Analytical solutions

The ideal PV staircase is a *piecewise constant* profile of potential vorticity extending from one hemisphere to the other, corresponding to a continuous, *piecewise linear* profile of absolute angular momentum. We consider exclusively profiles with even or odd symmetry about the equator having either an even (2, 4, 6 . . .) or odd (3, 5, 7 . . .) number of stair steps—a *step* corresponding to the flat (latitude invariant) part of the PV profile. The former profiles have a PV jump exactly on the equator and are in superrotation, with (prograde) equatorial westerlies; the latter have a middle step centered on the equator and may be in equatorial subrotation, with (retrograde) equatorial easterlies, or (somewhat less likely) in weak equatorial superrotation with two westerly jets straddling the equator. When cross equatorial symmetry is assumed, an odd number of steps requires trivially that the middle step be centered on the equator. The poleward extent of the PV staircase is regarded either as a parameter or variable of the problem. In general, the stair does not extend all the way to the poles, a scenario considered unlikely, as explained by Scott and Polvani (2007).

The absolute angular momentum is

$$m = a \cos\theta(\bar{u} + \Omega a \cos\theta), \quad (2.1)$$

where \bar{u} is the mean zonal wind, Ω and a are the rotation rate (positive eastward) and radius of the planet, respectively, and θ is latitude. The absolute vorticity—a surrogate for PV in the barotropic model—is

$$\bar{\zeta}_a = 2\Omega \sin\theta - \frac{1}{a \cos\theta} \frac{\partial}{\partial\theta}(\bar{u} \cos\theta). \quad (2.2)$$

These quantities are related as

$$\bar{\zeta}_a = -\frac{1}{a^2} \frac{\partial m}{\partial \mu}, \quad (2.3)$$

where $\mu = \sin\theta$. Hereafter we use nondimensional quantities

$$m = \Omega a^2 m^* \quad (2.4a)$$

$$\bar{\zeta}_a = \Omega \bar{\zeta}_a^* \quad (2.4b)$$

$$\bar{u} = \Omega a U \quad (2.4c)$$

such that

$$\bar{\zeta}_a^* = -\frac{\partial m^*}{\partial \mu}. \quad (2.5)$$

For notational convenience the asterisks are omitted from these symbols in the remainder of this section; unless indicated otherwise, the quantities m and $\bar{\zeta}_a$ are in nondimensional form.

a. Mode 0: Equatorial superrotation (single jet)

The resting atmosphere has $m = 1 - \mu^2$, a downward concave parabola in μ with maximum m on the equator, going to zero at the poles. A symmetric solution with equatorial superrotation can be obtained easily as

$$m = m_e \pm (1 - \mu_p^2 - m_e) \frac{\mu}{\mu_p}, \quad (2.6)$$

where $m_e \geq 1$ is the equatorial value of m and μ_p is the poleward terminus of the mixing zone. The minus sign is chosen for solutions in the “Southern” Hemisphere $\mu < 0$. This construction is illustrated in Fig. 1a. For conservation of absolute angular momentum we require that the areas bounded by the two curves are identical in the interval $[0, \mu_p]$:

$$m_e \mu_p + \frac{1}{2}(1 - \mu_p^2 - m_e)\mu_p = \mu_p - \frac{1}{3}\mu_p^3, \quad (2.7)$$

so that

$$\mu_p = \sqrt{3(m_e - 1)}. \quad (2.8)$$

Note that the integration is performed over μ , which accounts properly for the diminishing surface area as meridians converge to the poles. In this simple solution with a single prograde (westerly) jet on the equator (hereafter “mode 0”) a direct correspondence exists between the degree of equatorial superrotation ($m_e - 1$) and the poleward terminus of the mixing zone, μ_p . A maximum value of superrotation (1/3) is realized when

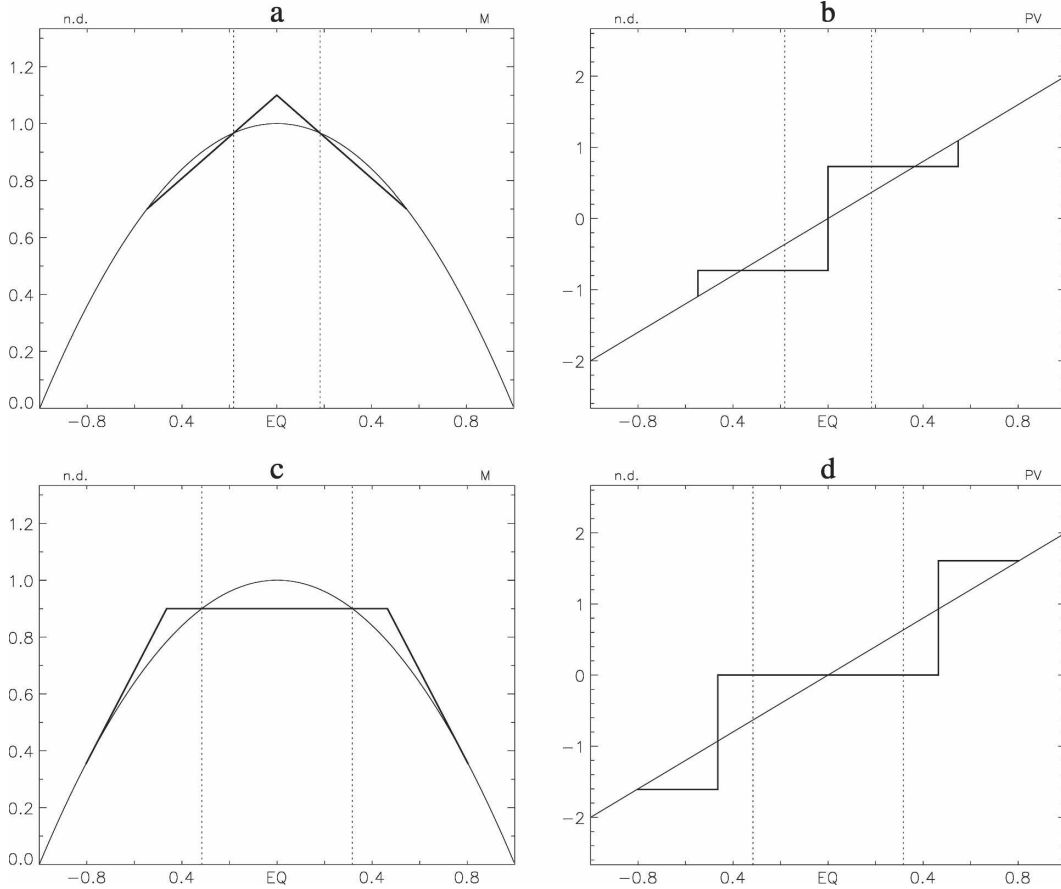


FIG. 1. (a) Angular momentum for mode 0 solution superposed on the resting parabola, plotted as a function of $\mu = \sin\theta$. Vertical dashed lines indicate latitudes where the angular momentum does not change between the resting and staircase states. (b) Same as in (a), but for PV. We refer to a *step* in the staircase as the flat (latitude invariant) part, and a *riser* as the sudden jump (positive northward). The integrated change of PV outside the dashed lines is identically zero by Stokes theorem. (c) Angular momentum as in (a), but for mode 1. In this special case of mode 1 the outer part of the staircase solution is constrained to be tangent to the resting parabola. (d) Potential vorticity as in (b), but for mode 1. The areas outside the vertical dashed lines circumscribed by the resting and staircase profiles of PV appear to be approximately the same and are, in fact, equal as required by Stokes theorem.

mixing extends over the entire hemisphere in both hemispheres ($\mu_p = 1$).

The absolute vorticity of the resting atmosphere is 2μ , and of the mixed atmosphere is

$$\begin{aligned} \bar{\zeta}_a &= \mp \frac{1}{\mu_p} (1 - \mu_p^2 - m_e) \\ &= \pm \frac{4}{3} \sqrt{3(m_e - 1)} \\ &= \pm \frac{4}{3} \mu_p. \end{aligned} \tag{2.9}$$

In the limiting case $\mu_p = 1$, $\bar{\zeta}_a = \pm 4/3$. Figure 1b illustrates the PV staircase for mode 0. This solution has the interesting property that the value of homogenized PV

in either hemisphere is greater (in absolute value) than a homogenized value obtained by mixing the hemispheres individually (± 1 for the limiting case). Evolution to the mixed state from an atmosphere initially at rest has required an upgradient transport of PV from the Southern to Northern Hemisphere in addition to the intrahemispheric mixing between the tropics and midlatitudes of each hemisphere.

As a check on self-consistency of the mode 0 solution we may calculate the time-integrated tendencies of (i) absolute angular momentum at the equator (the equatorial “impulse”) and (ii) absolute vorticity integrated over the Northern Hemisphere:

$$\Delta m_e = \Delta \langle \bar{\zeta}_a \rangle. \tag{2.10}$$

The change in equatorial m is obviously

$$\Delta m_e = m_e - 1 = \frac{1}{3} \mu_p^2, \quad (2.11)$$

while the initial and final values of hemisphere-integrated absolute vorticity inside $\pm\mu_p$ (it does not change outside) are

$$\langle \bar{\zeta}_a \rangle = \begin{cases} \int_0^{\mu_p} 2\mu \, d\mu & = \mu_p^2 & t = t_i, \\ -\int_0^{\mu_p} \frac{1}{\mu_p} (1 - \mu_p^2 - m_e) \, d\mu & = \frac{4}{3} \mu_p^2 & t = t_f. \end{cases} \quad (2.12)$$

The final and initial values of $\langle \bar{\zeta}_a \rangle$ differ by the amount on the rhs of (2.11), confirming (2.10). In other words, the equatorial impulse leading to superrotation is exactly consistent with the interhemispheric flux of PV leading to that state. This result illustrates (i) Stokes theorem applied to the entire hemisphere with a bounding contour lying on the equatorial latitude circle, and (ii) a generalized ‘‘Taylor identity’’ (Dunkerton 1980; Dritschel and McIntyre 2007) in which the acceleration along a fixed closed contour is determined by the flux of absolute vorticity across the contour. In Fig. 1b the impulse corresponds graphically to the change in PV between the equator and latitudes:

$$\pm\mu = \mu_0 = \frac{1}{2} \mu_m = \frac{1}{3} \mu_p, \quad (2.13)$$

where μ_0 —indicated by vertical dashed lines in Figs. 1a,b—is the (absolute value of) latitude where m does not change and μ_m is the midpoint of a ‘‘midlatitude’’ mixing zone lying beyond μ_0 . The change of PV integrated from the equator to μ_0 is geometrically

$$\frac{3}{4} \mu_0 \frac{4}{3} \mu_p = \frac{1}{3} \mu_p^2 = m_e - 1 = \Delta m_e. \quad (2.14)$$

Note that the meridionally and time-integrated absolute vorticity tendency outside $\pm\mu_0$ is zero since the changes straddling $\pm\mu_m$ are equal and opposite. Stokes theorem applied on partial hemispheres poleward of $\pm\mu_0$ therefore implies no net change of absolute angular momentum (or of mean zonal velocity) on the bounding latitude circles $\pm\mu_0$, consistent with Fig. 1a.

Although nothing has been said about transport mechanisms, the meridional transport of angular momentum and potential vorticity by eddies is presumably required for equatorial superrotation. The tendency of mean zonal wind can be written (in dimensional form)

either in terms of the meridional convergence of eddy momentum flux, or (using the Taylor identity) as

$$\frac{\partial \bar{u}}{\partial t} = \overline{v' \zeta'} \quad (2.15a)$$

$$\frac{\partial m}{\partial t} = a \cos \theta \overline{v' \zeta'}. \quad (2.15b)$$

The tendency of mean relative vorticity is

$$\frac{\partial \bar{\zeta}}{\partial t} = -\frac{\partial}{\partial \mu} \left(\overline{v' \zeta'} \frac{\cos \theta}{a} \right). \quad (2.16)$$

Advection by a mean meridional circulation is neglected, consistent with the barotropic model. The tendencies of m and $\bar{\zeta}$ are consistent with (2.3), noting that the planetary component of $\bar{\zeta}_a$ does not change with time.

Eddy mixing processes are necessary for staircase formation, and some combination of ‘‘interhemispheric’’ and ‘‘intra-hemispheric’’ PV transport is also required. Knowledge of the initial and final state alone, however, is insufficient to choose one mixing scenario over another. Rather, we note a valuable lesson from this example: in the absence of external forcings and mean meridional circulation, transport of PV across (what is to become ultimately) a ‘‘barrier’’ to meridional transport by breaking Rossby waves and instabilities is necessary in order to set up the barrier in the first place. This fact has an important implication for the construction of general solutions in section 2c.

b. Mode 1: Equatorial sub- and superrotation (twin jets)

A solution with three mixing zones can be obtained easily, with $m = m_e = \text{constant}$ from the equator to some latitude $\pm\mu_1$ and

$$m = m_e + \frac{|\mu| - \mu_1}{\mu_p - \mu_1} (1 - \mu_p^2 - m_e) \quad (2.17)$$

in the interval $\pm[\mu_1, \mu_p]$. This construction is shown in Fig. 1c. Conservation of absolute angular momentum requires that

$$\begin{aligned} m_e \mu_p + \frac{1 - \mu_p^2 - m_e}{\mu_p - \mu_1} \left[\frac{1}{2} \mu^2 - \mu \mu_1 \right]_{\mu_1}^{\mu_p} \\ = m_e \mu_p + \frac{1}{2} (1 - \mu_p^2 - m_e) (\mu_p - \mu_1) \\ = m_e \mu_1 + \frac{1}{2} (m_1 + m_p) (\mu_p - \mu_1) = \mu_p - \frac{1}{3} \mu_p^3, \end{aligned} \quad (2.18)$$

where $m_1 = m(\mu_1) = m_e$ and $m_p = m(\mu_p) = 1 - \mu_p^2$. The second term on the last line of (2.18) represents intuitively the average angular momentum in the outer mixing zone multiplied by the width of the zone. This equivalence is valid for any linear-in- m segment of the staircase.

The absolute vorticity (Fig. 1d) is zero in the middle zone straddling the equator and is equal to

$$\bar{\zeta}_a = \mp \frac{(1 - \mu_p^2 - m_e)}{\mu_p - \mu_1} \quad (2.19)$$

in the interval $\pm[\mu_1, \mu_p]$, where the lower (positive) sign once again is selected for the Southern Hemisphere. The mode 1 solution is underdetermined, with two variables, μ_1 and μ_p (for a given m_e), but only one angular momentum constraint. A limiting case of marginal stability can be obtained, nevertheless, as shown in Fig. 1d by assuming that the absolute vorticity is continuous at $\pm\mu_p$:

$$2\mu_p = - \frac{1 - \mu_p^2 - m_e}{\mu_p - \mu_1}. \quad (2.20)$$

It is a limiting case in the sense that, if the absolute vorticity were lower (in absolute value) outside of $\pm\mu_p$ than inside, the flow would be barotropically unstable in the neighborhood of $\pm\mu_p$ and would presumably remove the instability, returning m and $\bar{\zeta}_a$ to their limiting profiles. This assumption corresponds graphically in Fig. 1c to the requirement that the slope of m in the midlatitude mixing zone not exceed the slope of the resting profile at μ_p , that is, that the straight segment is tangent to the parabola. This situation also yields the largest possible reduction of m_e below 1, that is, equatorial subrotation.

The two constraints (2.18) and (2.20) provide two relationships for m_e :

$$1 - m_e = \frac{1}{3} \mu_p^2 - (\mu_p - \mu_1)^2 \quad (2.21a)$$

$$1 - m_e = \mu_p^2 - 2\mu_p(\mu_p - \mu_1) \quad (2.21b)$$

so that

$$\mu_p^2 = 3\mu_1^2 \quad (2.22a)$$

$$1 - m_e = \mu_1^2(2\sqrt{3} - 3) \quad (2.22b)$$

$$3(1 - m_e) = \mu_p^2(2\sqrt{3} - 3). \quad (2.22c)$$

The last equality, (2.22c), provides a unique relationship between m_e and μ_p analogous to (2.8). As in the mode 0 solution it is easy to verify that the equatorial impulse starting from an atmosphere at rest, $\Delta m_e = \mu_1^2(3 - 2\sqrt{3})$, is exactly consistent with a downgradient

cross-equatorial transport of absolute vorticity from the Northern to Southern Hemisphere. Once again we may imagine that the net transport is equivalent to a homogenization of absolute vorticity in the interval $[-\mu_0, \mu_0]$, where

$$\mu_0 = \mu_1 \sqrt{2\sqrt{3} - 3} = \sqrt{1 - m_e}, \quad (2.23)$$

while the remaining mixing outside μ_0 is intrahemispheric only. The mean flow is unchanged at $\pm\mu_0$, and the integrated absolute vorticity outside this latitude is also unchanged, as required by Stokes theorem.

It is fortuitous that the limiting (marginally stable) mode 1 solution displays only two jets (Fig. 1c) or “risers” of the PV staircase (Fig. 1d) from pole to pole whereas the mode 0 solution contains three risers (Fig. 1b). In fact the mode 1 solution should always be regarded as having four risers; it just happens that the PV jumps at $\pm\mu_p$ are identically zero in this limit. The general form of the mode 1 solution is a barotropically stable configuration with easterlies poleward of the jets at $\pm\mu_1$ extending from $\pm\mu_0$ to $\pm\mu_p$. Three examples are shown in Figs. 2a,c,e. The angular momentum constraint is given by (2.18), but barotropic stability at $\pm\mu_p$ requires that

$$2\mu_p \geq - \frac{(1 - \mu_p^2 - m_e)}{\mu_p - \mu_1}. \quad (2.24)$$

The corresponding profiles of absolute vorticity are shown in Figs. 2b,d,f. The first example displays weak equatorial superrotation with a pair of off-equatorial prograde jets. Mode 0 is evidently a limiting form of the superrotating mode 1 solution when these off-equatorial jets collapse to a single on-equatorial jet. In such superrotating cases the equatorial stair step is narrower than the other two midlatitude steps. In between the subrotating and weakly superrotating solutions is another special case (Figs. 2c,d) obtained by setting $m_e = 1$. The steps of the PV staircase are of equal width in this case. The tropical part of this angular momentum-conserving (AMC) solution was obtained by Held and Hou (1980) in the upper troposphere for heating symmetric about the equator. In this special case

$$\mu_1 = \frac{1}{3} \mu_p \quad (2.25a)$$

$$\mu_0 = \frac{1}{2} \mu_p \quad (2.25b)$$

and

$$\bar{\zeta}_a = \pm \frac{3}{2} \mu_p \quad (2.26)$$

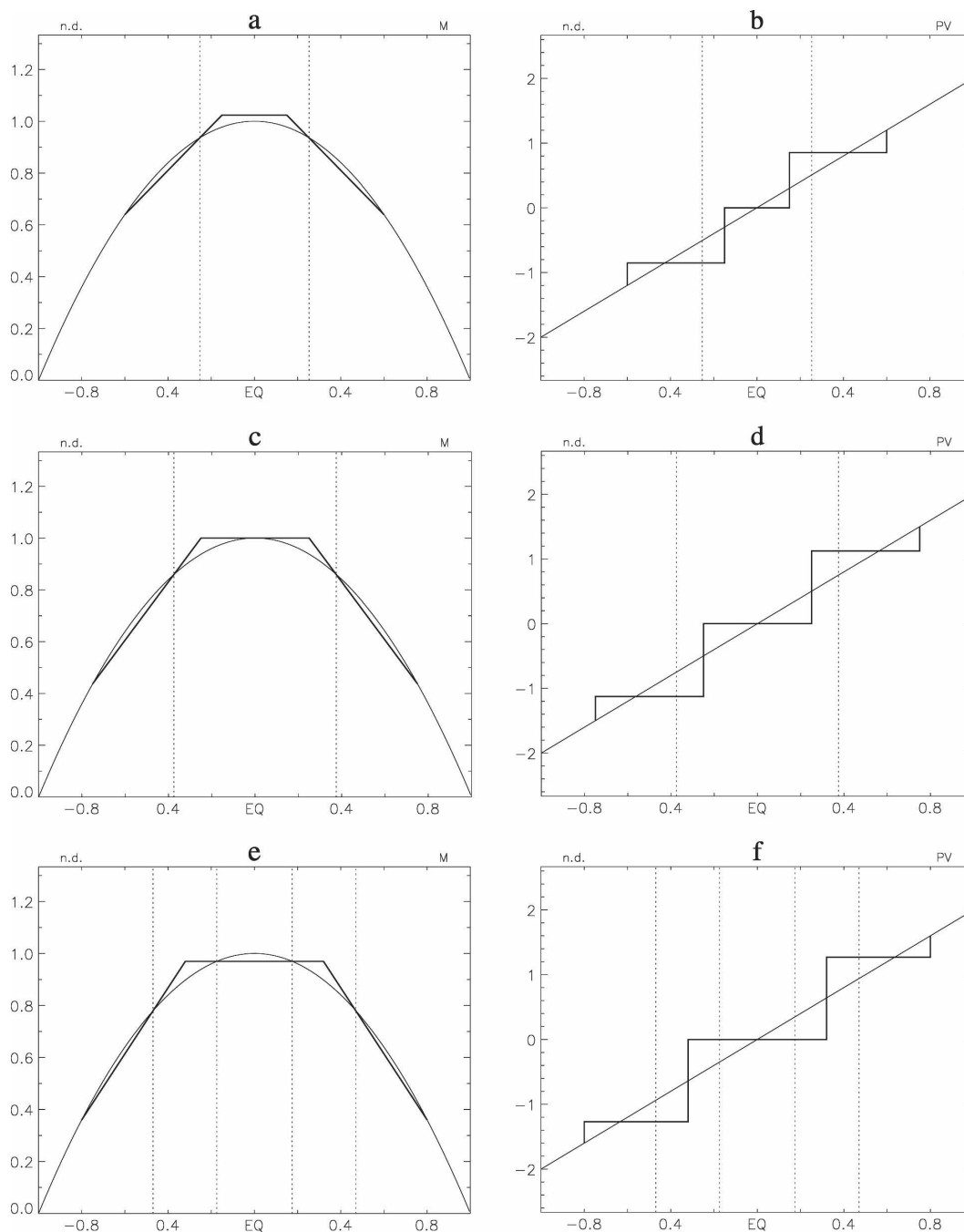


FIG. 2. Angular momentum and potential vorticity as in Fig. 1, but for mode 1 solutions with (a), (b) $\mu_p = 0.6$, $x \equiv \mu_1/\mu_p = 0.25$, (c), (d) $\mu_p = 0.75$, $x = 0.3333$, and (e), (f) $\mu_p = 0.8$, $x = 0.4$. Note in (e) that the subrotating solution has two pairs of latitudes where the change of angular momentum between resting and staircase states is zero.

in the interval $\pm[\mu_1, \mu_p]$, which may be compared to its value $\pm 2\mu_p$ in the limiting case of marginal stability. Unlike the preceding cases, there is no unique relationship between m_e and μ_p in (2.25) and (2.26) since any value of μ_p is possible in this *self-similar* solution. The

final example shown in Figs. 2e,f is in equatorial subrotation with small risers at $\pm\mu_p$. In this case the equatorial stair-step is the widest of the three, and a second pair of μ_0 exist near the equator.

The axisymmetric model of Held and Hou did not

allow eddy mixing outside of μ_1 ; absolute angular momentum instead was advected downward in the subsiding branch of the Hadley circulation, ultimately returned to the solid Earth in a (frictionally controlled) surface return flow. Our barotropic model of eddy mixing on the sphere is very different from their model of the axisymmetric and equatorially symmetric Hadley circulation but shares the same property, when $m_e = 1$, of zero exchange of angular momentum and PV between hemispheres. This special case has zero impulse at the equator and therefore no change in meridionally integrated absolute vorticity in each hemisphere individually. Of the examples shown, $m_e = 1$ marks the boundary between upgradient and downgradient PV transport across the equator.

We note finally that the general form of mode 1 solution (including the mode 0 solution as a limit) is embraced by the relationship

$$\Delta m_e = m_e - 1 = \mu_p^2 \frac{1/3 - x}{1 + x} \tag{2.27a}$$

$$\bar{\zeta}_a = \pm \frac{4}{3} \mu_p \frac{1}{1 - x^2}, \tag{2.27b}$$

where $\mu_1 \equiv x\mu_p$. The three special cases highlighted in Figs. 1a,b, 2c,d and 1c,d, respectively, are (i) mode 0 limit ($x = 0$), (ii) Held and Hou (1980) AMC circulation ($x = 1/3$), and (iii) limit of marginally stable flow at $\pm\mu_p$ ($x = 1/\sqrt{3}$). The latitudes of zero impulse are given by the solution of a quadratic equation in x' with coefficients

$$a = 1 - x^2 \tag{2.28a}$$

$$b = -\frac{4}{3} \tag{2.28b}$$

$$c = \frac{1}{3} + x^2, \tag{2.28c}$$

where $\mu_0 \equiv x'\mu_p$. This result is validated by the vertical dashed lines in Fig. 2, and it can be shown analytically that the correct values are obtained using this formula in the special cases highlighted above. The negative root yields the vertical dashed lines, whereas the positive root corresponds trivially to $x' = 1$ (not shown). The trivial solution is obtained from the fact that $a + b + c = 0$. Using this condition, the negative root of the quadratic formula simplifies to the remarkable equality

$$\bar{\zeta}_a = \mu_0 + \mu_p, \tag{2.29}$$

which can be visualized, in geometric terms, from the plots of absolute vorticity in the following way. The change of meridionally integrated absolute vorticity is identically zero outside μ_0 (as required by Stokes theorem, since μ_0 is the latitude where the mean flow does not change), implying that the two small triangles in this region formed by the intersection of the initial and final linear segments of $\bar{\zeta}_a$ are identical. Hence

$$\bar{\zeta}_a - 2\mu_0 = 2\mu_p - \bar{\zeta}_a, \tag{2.30}$$

whereupon (2.29) follows. The extra pair of dashed lines in Figs. 2e,f originates from (2.23) in cases where $\Delta m_e < 0$.

From the preceding discussion it is clear that Stokes theorem constrains the area of adjacent polygons—formed by the intersection of initial and final profiles of $\bar{\zeta}_a$ and bounded laterally by any of the possible values of μ_0 —to be equal, ensuring that the meridionally integrated absolute vorticity does not change in such regions. Our illustrated cases afford three additional examples of equal-area polygon pairs as follows: (i) in Fig. 1d, a rhomboid and triangle, equatorward and poleward of μ_1 ; (ii) in Fig. 2d, a triangle and rhomboid, equatorward and poleward of μ_1 ; and (iii) in Fig. 2f, the two rhomboids straddling μ_1 . (In the latter example, despite appearances, μ_1 does *not* lie exactly midway between the two values of μ_0 ; nevertheless, the rhomboids have equal area.) The reader may verify that the polygons in each pair have equal area by substituting the arithmetic values of μ_0 , μ_1 , and μ_p in each case.

The process of building a PV staircase from the initial linear slope 2μ may be likened to the construction of terraces on a linear grade where the soil, like PV, is a conserved quantity. The same end result can be achieved by any number of mixing scenarios. As noted in section 2a, we are inclined to choose the simplest rearrangement as the most likely; however, without additional information on mixing processes, there is no reason to select one scenario over another. Consider the challenge posed by Fig. 2b, the weak superrotating mode 1 solution. In this case, the simplest rearrangement of soil (in other words, PV) transfers the rhomboidal section equatorward of $-\mu_0$ in the Southern Hemisphere to its new location equatorward of $+\mu_0$ in the Northern Hemisphere, while flattening the equatorial grade in the opposite direction by flipping the triangular section just north of the equator to the southern side. An alternative scenario leaves behind a small portion of the rhomboid to fill in the triangle south of the equator, and then picks up additional soil just north

of the equator on the way to forming the northern wall. Putting this in the context of the dynamics of a rotating fluid, the first scenario requires *nonlocal mixing*, in the sense that lateral eddy scales increase linearly from the equator, while the second scenario suggests a more uniformly *local mixing* process across the tropical belt. Nonlocal mixing is uncharacteristic of Fickian diffusion but is possible in the general framework of “transilient turbulence” described by Stull (1984). The formation of prograde (westerly) jets in our illustrations requires (i) positive (upgradient) PV transport [cf. (2.10a) and (2.10b)] and (ii) inhomogeneous mixing, with PV homogenization restricted to mixing zones between the jets (McIntyre 1982; McIntyre and Palmer 1983).

c. Higher modes with cross-equatorial symmetry

Unlike the mode 0 solution, for which a unique relationship exists between the degree of equatorial superrotation Δm_e and adjacent mixing zones, the mode 1 solution and all higher solutions are underdetermined when angular momentum conservation provides the only constraint on the problem. Because of their infinite number and variety, it seems pointless to discuss higher-mode solutions without invoking additional constraints that, in effect, select unique combinations of profile parameters. In this subsection our procedure is to select a mode number (i.e., a given number of steps and risers) and then determine combinations of profile parameters that satisfy the imposed constraints. The two hemispheres are assumed symmetric in m . The convention is that *even* modes $n = 0, 2, 4 \dots$ have a *jet* on the equator while *odd* modes $n = 1, 3, 5 \dots$ have a *stair step* centered on the equator. Going from one even n to the next, a new jet is added in each hemisphere, which introduces two new variables: namely, the position and strength of the jet. The same occurs going from one odd n to the next. (An even mode may be regarded as having the same number of jets in each hemisphere as the following odd mode, but with the two jets closest to the equator collapsed into one.) We infer that for each new jet in the Northern Hemisphere, two additional constraints must be imposed in order to preserve a unique functional relationship between m_e and μ_p . To understand this requirement in more detail, the global angular momentum constraint for mode number n may be written (in each hemisphere) as

$$\sum_{j=0}^N \frac{1}{2} (m_j + m_{j+1}) \frac{1}{2} (\delta\mu_j + \delta\mu_{j+1}) = \mu_p - \frac{1}{3} \mu_p^3, \tag{2.31}$$

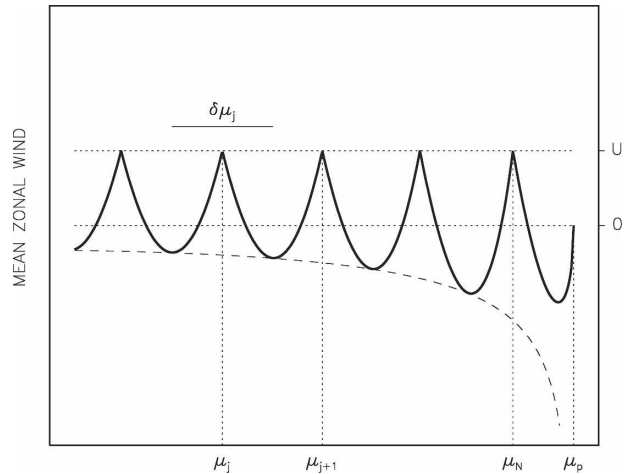


FIG. 3. Construction of PV staircase for higher mode numbers (in this case, mode 10, with $p = -0.08$) illustrating a variable spacing of constant prograde (westerly) jets, slight increase of easterly jet amplitude approaching the pole, and a polar anticyclone formally lying outside the staircase. When $p > 0$ ($p < 0$), jet spacing increases (decreases) in μ approaching the pole. The jet spacing increases in θ in either case if $p > -0.5$. The example shown lies near the coalescence point and has weak polar easterlies. On the interior branch above this point, the polar flow becomes westerly.

where $N = (n + 1)/2$ and $\delta\mu_j$ is the spacing, between prograde (westerly) jets, associated with the j th jet located at μ_j . Figure 3 illustrates the staircase construction just described. This expression generalizes the last line of (2.18) to an arbitrary number of steps. The convention is that $j = 0$ is located on the equator (regardless of even or odd symmetry) and $j = N + 1$ is the outermost riser at μ_p . For the outer boundary condition

$$m_{N+1} = 1 - \mu_p^2 \tag{2.32a}$$

$$\frac{1}{2} (\delta\mu_N + \delta\mu_{N+1}) \rightarrow \mu_p - \mu_N \tag{2.32b}$$

so that the outermost riser is not a westerly jet; rather, it is a point of intersection with the resting parabola. In (2.31) there are $2(N + 2)$ “basic variables” $m_j, \delta\mu_j$ —from which it is again apparent that two new variables are introduced with each increment of N . The average angular momentum in each mixing zone is multiplied by the width of that zone [cf. (2.18)] and we imagine that the width of each mixing zone is determined somehow by the two jets bounding that zone. We regard (2.31) as a *global* constraint; that is, we do not require angular momentum to be *conserved locally* in individual mixing zones. This expectation is consistent, at least, with the realization that jet formation, if attributable to eddies, requires an eddy flux of potential vor-

ticity across the latitude of the jet during its period of formation.

Aside from the spherical geometry and global angular momentum constraint, all of the geophysical fluid dynamics (GFD; wave and instability momentum transport and turbulent mixing processes) is contained in the specification of m_j and $\delta\mu_j$. This is by no means a trivial problem, and we wish to make clear that the following discussion is not intended to solve fully the dynamical problem, but to illustrate how—with certain simplifying but reasonable assumptions—the spherical geometry and global angular momentum constraint may be used to construct ideal PV staircases with $n \geq 2$ in much the same way as done with the lowest two modes illustrated in sections 2a, b. Toward this end, two constraining formulas are introduced that are based loosely on the numerical results of Scott and Polvani (2007):

1) JET STRENGTH

The maximum speed of prograde (westerly) jets is approximately constant across the staircase when the radius of deformation is greater than or equal to the planetary radius.²

Therefore

$$m_j - m_j(0) = U \sqrt{1 - \mu_j^2} \quad \text{for } j = 0, 1 \dots N, \quad (2.33)$$

where U is the maximum mean zonal wind (\bar{u}) of each jet, scaled by Ωa , and $m_j(0)$ denotes the absolute angular momentum of the resting atmosphere. The observed uniformity of U suggests that eddy potential vorticity fluxes are reasonably constant across the sphere (at jet latitudes) when the deformation radius L_D is large; that is, when the waves and eddies responsible for the transport are not equatorially confined. We note incidentally that the assumption of uniform jet strength is a safe bet on the midlatitude β plane (Danilov and Gurarie 2004) with constant β . This symmetry is broken on the sphere, with its variable β (and variable deformation radius). Notwithstanding this complication, multiple jets on the sphere are remarkably similar at large L_D .

2) JET SPACING

The number of jets in the staircase is inversely proportional to a Rhines scale as determined by the rms value of zonal wind (dominated by the zonal mean or “jet” component) as well as an “energy centroid” in the

spherical wavenumber spectrum of kinetic energy (also dominated by the zonal-mean zonal component). For large deformation radius L_D , we assume that

$$\delta\mu_j^{-1} = C \sqrt{\frac{F(\beta)}{2U}} = C(1 - \mu^2)^p / \sqrt{U} \quad \text{for} \\ j = 0, 1 \dots N, \quad (2.34)$$

where $\beta = 2\sqrt{1 - \mu^2}$ is the nondimensional planetary vorticity gradient, scaled by Ω/a . When $F(\beta) = \beta$, $p = 1/4$, noting that β varies as cosine of latitude; this is the familiar “Rhines scale” derived from the Rossby wave dispersion relation on the midlatitude β plane. There is evidently some uncertainty on how to apply the Rhines scale in a spherical domain. On the one hand, a *global* type of disturbance (e.g., a Rossby–Haurwitz wave) suggests that we consider individual wavelengths and jets with roughly equal spacing in μ . This choice would be motivated by the latitudinal structure of Rossby–Haurwitz waves as Legendre functions. On the other hand, a *local* view of waves and their interaction with jets (or a local view of turbulence in a sheared flow) suggests that we consider jet spacings that vary in θ , with some expansion or contraction in μ approaching the poles. This choice would involve the application of Rhines scaling, appropriate for the midlatitude β plane, to all latitudes. At this point a specific choice is not needed, only that the range of choices is plausible. It will prove illuminating to consider three values of p ranging from $1/4$ to $-1/4$, corresponding, respectively, to jet spacings (i) that expand slowly in the μ coordinate, approaching the poles, (ii) that are equally spaced in μ , and (iii) that contract slowly in the μ coordinate, approaching the poles. It is very important to note that in all three cases there is a slow expansion of jet spacing with latitude when viewed in the θ coordinate. There is no need to consider equal jet spacing in *latitude* since the simulated jet spacing always increases approaching the pole (usually attributed to the variation of β). For simplicity, the parameter C is taken to be uniform, recognizing that transport processes are similar across the staircase when the deformation radius is large. The effects of small L_D in the shallow-water system are discussed in the sequel. It is unlikely that a universal value of C exists; this parameter almost certainly depends on model setup (e.g., how the flow is forced) and the ability or otherwise of adjacent jets to persist when interleaved with mixing zones. From Scott and Polvani (2007) we infer that $C \sim 0.3$ over four orders of magnitude of forcing strength (the dependence of spacing on L_D is weak), whereas for the ideal mode 0 and 1 staircases shown here, $C = O(1)$. It will be instructive to examine values of C lying in this range.

² For a small deformation radius this constraint does not apply: jet strength decreases with latitude, and we regard polar regions, with their isotropic turbulence, as formally outside the staircase.

The parameters C , U , and μ_p may be regarded as “auxiliary” variables when enough constraints are imposed to determine them. With the current inventory of equations and variables we are required to specify two of the three auxiliary variables as parameters, from which the third auxiliary variable may be determined as part of the solution. Here, C and U will be specified and μ_p will be determined by the angular momentum constraint once all of the μ_j are obtained from

$$\mu_{j+1} = \mu_j + \frac{1}{2}(\delta\mu_j + \delta\mu_{j+1}) \quad \text{for } j = 0, 1 \dots N - 1. \tag{2.35}$$

For the μ_j , one needs only to specify a ratio of parameters U/C^2 [cf. (2.34)]. However, it is not possible to absorb C completely in the definition of U because C does not appear explicitly (in the ratio U/C^2) in the definition of angular momentum (2.33).

With our simplifying constraints the mode 2 solution ($N = 1$) is determined by

$$m_0 = m(U, \mu_0) = 1 + U \tag{2.36a}$$

$$m_1 = m(U, \mu_1) = 1 - \mu_1^2 + U\sqrt{1 - \mu_1^2} \tag{2.36b}$$

$$m_2 = 1 - \mu_2^2 \tag{2.36c}$$

$$\mu_0 = 0 \tag{2.36d}$$

$$\mu_1 = \mu_0 + \frac{1}{2}(\delta\mu_0 + \delta\mu_1) \tag{2.36e}$$

$$\mu_2 = \mu_p, \tag{2.36f}$$

together with (2.34) for the $\delta\mu_j$ and subject to the global angular momentum constraint

$$\sum_{j=0}^1 \frac{1}{2}(m_j + m_{j+1})(\mu_{j+1} - \mu_j) = \mu_p \left(1 - \frac{1}{3}\mu_p^2\right). \tag{2.37}$$

An example is shown in Fig. 4, with $C = 0.42$, $U = 0.043$, and $p = 1/4$. In this case the outer mixing zones are almost tangent to the resting parabola (Fig. 4a); only tiny risers remain at $\pm\mu_p$ (Fig. 4b), which could be easily eliminated with a small change of parameters. The equatorial riser is slightly stronger than the middle risers at $\pm\mu_1$, owing to a more acute angle of m at the equator. Redistribution of absolute angular momentum

occurs mainly between the westerly jets at $\pm\mu_1$ and the tropical interior, with its equatorial westerly jet and flanking easterlies. The first three terms of a Taylor series (introduced in section 2e) are an excellent approximation of the exact values at $\pm\mu_1$ (Figs. 4c,d). These jets are separated from the equatorial jet by significant easterlies (Fig. 4e)—a consequence of the interior redistribution of m , as opposed to an exterior redistribution, which would create significant easterlies extending to $\pm\mu_p$, complemented by stronger tropical westerlies (see below). Global conservation of absolute angular momentum is illustrated by the change of relative angular momentum (Fig. 4f) providing a more lucid view of this constraint than shown by the change of absolute angular momentum (Fig. 4a).

An example of mode 3 is shown in Fig. 5, determined by

$$m_0 = m_1 \tag{2.38a}$$

$$m_1 = m(U, \mu_1) = 1 - \mu_1^2 + U\sqrt{1 - \mu_1^2} \tag{2.38b}$$

$$m_2 = m(U, \mu_2) = 1 - \mu_2^2 + U\sqrt{1 - \mu_2^2} \tag{2.38c}$$

$$m_3 = 1 - \mu_p^2 \tag{2.38d}$$

$$\mu_0 = 0 \tag{2.38e}$$

$$\mu_1 = \mu_0 + \frac{1}{2}\delta\mu_1 \tag{2.38f}$$

$$\mu_2 = \mu_1 + \frac{1}{2}(\delta\mu_1 + \delta\mu_2) \tag{2.38g}$$

$$\mu_3 = \mu_p, \tag{2.38h}$$

again using (2.34) for the $\delta\mu_j$ and subject to the angular momentum constraint

$$\sum_{j=0}^2 \frac{1}{2}(m_j + m_{j+1})(\mu_{j+1} - \mu_j) = \mu_p \left(1 - \frac{1}{3}\mu_p^2\right). \tag{2.39}$$

There is no equatorial jet for the odd mode; consequently, only the half contribution from $\delta\mu_1$ is used in (2.38f), which determines μ_1 entirely. The parameters in Fig. 5 are $C = 0.4231$, $U = 0.039$, and $p = 0$. This example displays features similar to those of Fig. 4:

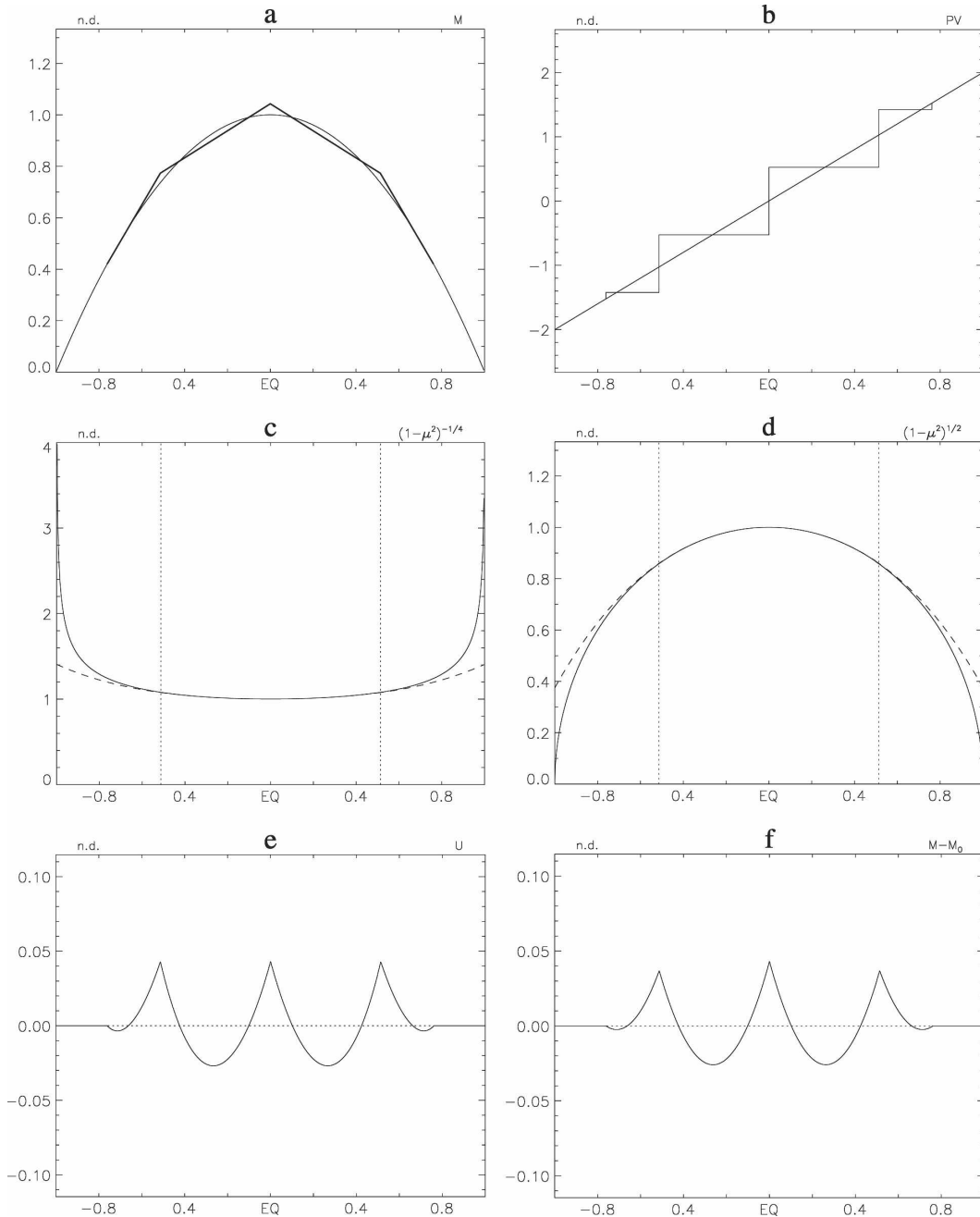


FIG. 4. Illustration of mode 2 solution (see text for parameter values): (a) angular momentum superposed on the resting parabola, (b) PV staircase with tiny risers at $\pm\mu_p$, (c) $(1 - \mu^2)^{-1/4}$ and its three-term Taylor series representation (dashed curve), (d) $(1 - \mu^2)^{1/2}$ and its three-term Taylor series representation (dashed curve), (e) relative zonal wind, and (f) relative angular momentum.

nearly tangent edges, interior redistribution of m , and taller risers near the equator (Figs. 5a,b). The Taylor series with three terms are accurate even at $\pm\mu_2$ (Figs. 5c,d). This example, unlike the previous one, has equatorial subrotation (retrograde easterlies). Equatorial easterlies are slightly weaker than in the midlatitudes

(Fig. 5e), which we attribute in general to (i) the different moment arms and (ii) the dependence of the Rhines scale on latitude. A measure of the latter effect can be seen in the slightly wider spacing of midlatitude jets when $p = 1/4$ (not shown). When $p = 0$, the variable spacing is eliminated, and the change of relative

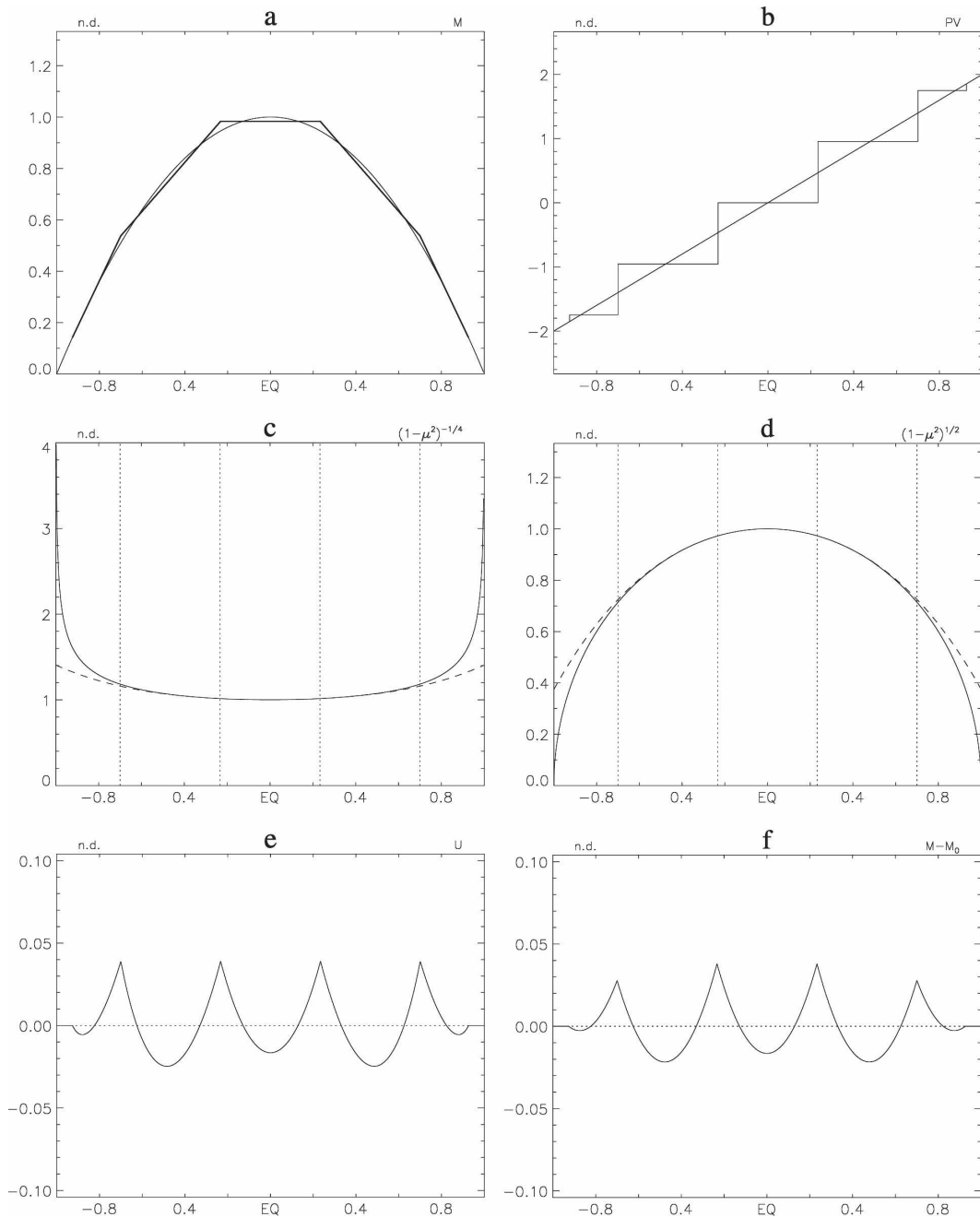


FIG. 5. Same as in Fig. 4, but for mode 3 solution (see text for parameter values).

angular momentum once again illustrates the global conservation of this invariant (Fig. 5f).

d. Parameter dependence

The meridional extent of the staircase μ_p and width of steps $\delta\mu_j$ generally increase with U up to a certain point, given C . Discussion of the parameter space therefore can be streamlined by considering the value

of U that maximizes μ_p subject to the geometric constraint $\mu_p \leq 1$. For exterior solutions this limit implies $\mu_p = 1$, whereas for interior solutions the staircase may or may not reach the pole depending on whether the values of C and U lie above or below a coalescence point, as illustrated in Figs. 6 and 7 for modes 2 and 3, respectively. As noted above (in connection with Fig. 4) angular momentum in the *exterior* solution is ex-

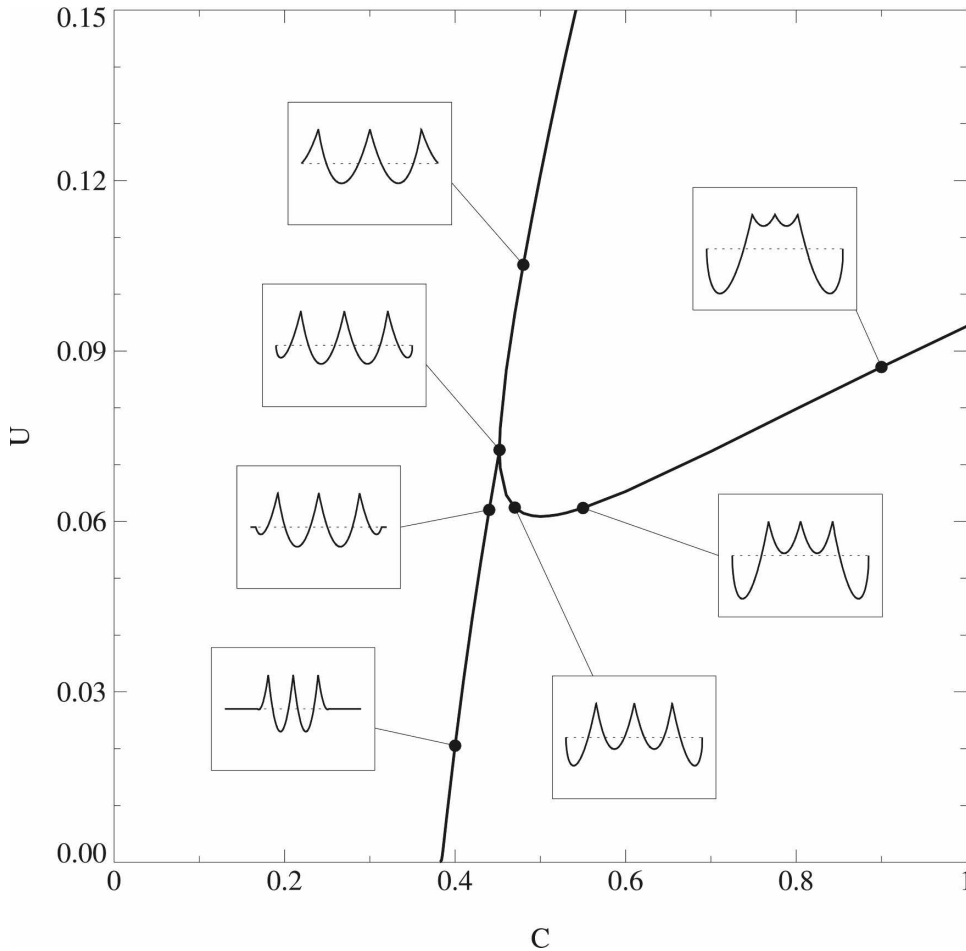


FIG. 6. Values of U as a function of C for mode 2 (with $p = 1/4$) that maximize μ_p as a function of U . Small panels inlaid show latitudinal profiles of relative zonal wind.

changed between the polar latitudes and the staircase itself, whereas for *interior* solutions these exchanges occur entirely between staircase steps. (Our terminology is unrelated to the interior and exterior solutions of Laplace’s equation in electrostatics.) Solution trajectories are similar for the two modes, although the maximum zonal wind is necessarily smaller in the mode 3 solution by about a factor of 2 in order to accommodate the additional jet. The thumbnails in each panel illustrate the jet structure in each of the three branches.³ For the interior solution the meridional width shrinks rapidly to zero when C is decreased below the coales-

cence point. In this branch, the staircase “rides the parabola” to its top very quickly as $U \rightarrow 0$ and C tends to a limiting value (since the mode number is fixed). By contrast, the exterior solution to the right of the coalescence point varies rather slowly with C , evidently because the outermost easterlies can be adjusted to accommodate variations in the tropical westerlies as U is changed. This adjustment presumably continues until a limiting structure resembling mode 0 is obtained, but with a sequence of steps near the equator. Above the coalescence point the interior solution develops polar westerlies associated with the outermost jets. The most interesting result of Figs. 6 and 7 is that a practical minimum of C exists for each mode, and this limit is almost identical for the two modes. It is evidently impossible to build a PV staircase of modes 2 or 3 at smaller C .

A simple argument explains why the constant of proportionality (C^{-1}) describing the ratio of jet spacing to

³ The branches shown maximize μ_p versus U for a particular C . A fourth branch may be defined below the lowest point of the exterior solution that maximizes μ_p versus C for a particular U . This branch (not shown) represents the asymptotic form of the exterior solution, just as the branch below the coalescence point represents the asymptotic form of the interior solution.

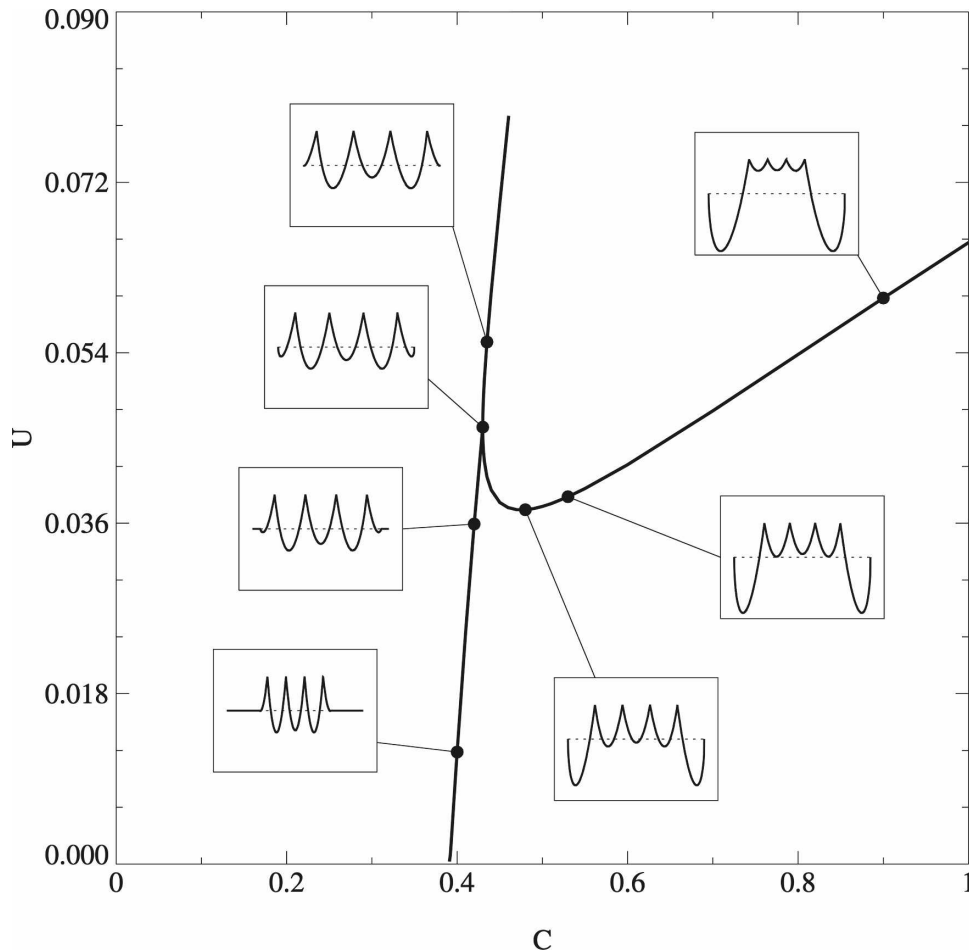


FIG. 7. Same as in Fig. 6, but for mode 3, with $p = 0$.

jet strength cannot exceed a critical value. Small U implies that (prograde) westerly jets form *small peaks* on top of the resting parabola, connected by linear-in- m segments with (retrograde) easterlies in their center. Large jet spacings, on the other hand, imply *large negative deviations* of retrograde segments below the resting parabola: *large*, that is, *if the westerly peaks are small*. The resulting discrepancy between small maximum westerly and large maximum easterly winds violates the global conservation of absolute angular momentum. For equal area of (the sum of all) westerly peaks and easterly valleys relative to the resting parabola, the linear segments must be sufficiently narrow in latitude. For fixed mode number n , the meridional extent of the staircase must therefore shrink to zero as $U \rightarrow 0$. When viewed in m , the PV staircase may be likened to a “necklace of bamboo” created from several small linear pieces of material. To preserve the curvilinear appearance of the necklace one must use either a few short pieces (analogous to small n) lying at the lowermost

point of the necklace when worn, or many short pieces (analogous to large n) filling the necklace from one end to the other. Deviations from the unfinished layout (without bamboo) thereby remain small in either case.

A slightly simpler model of the PV staircase regards the jet spacing as constant in μ . This special case is obtained by truncating (2.40b) to its leading term. Figures 8a,b illustrate solution trajectories for modes 2 and 3 when the effect of variable β is removed from the Rhines scaling (2.34). Results with $p = 0$ (thick curve) are similar to the more general cases $p = \pm 1/4$ (thin curves). This simplification establishes that the Rhines-scale concept (with a suitable scale factor C) is relevant not only to the construction of PV staircases on the sphere, but alternatively can be derived from the staircase solution assuming only that the jets are approximately equally spaced. Thus, we obtain a geometric Rhines scale, determined entirely by the constraints of angular momentum conservation and baro-

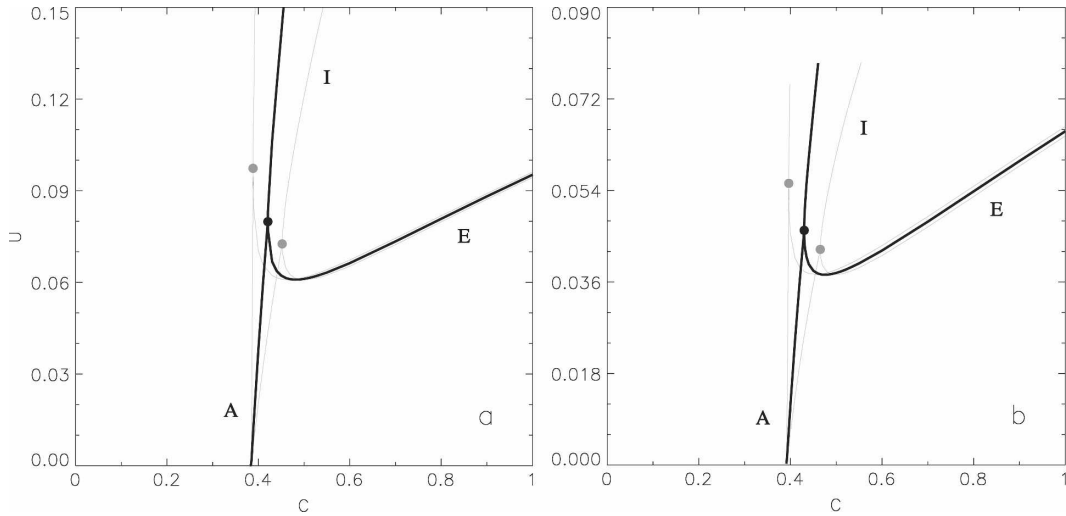


FIG. 8. Same as in Fig. 6, but comparing the solution trajectory for constant μ spacing of westerly jets ($p = 0$, thick line) with that for Rhines scaling in μ ($p = 1/4$, thin line at right) or θ (thin line at left) for (a) mode 2 and (b) mode 3. The inlays in Figs. 6 and 7 indicate the nature of solution branches, here labeled E (exterior), I (interior), and A (asymptotic).

tropic stability, which is independent of any assumption of wave transport processes or turbulence phenomenology.

The analytical model is easily extended to higher mode numbers. Figures 9a,b show the solutions for U (that maximize μ_p) for modes 4 and 5, respectively. Aside from their smaller wind magnitude, these curves are similar to those of modes 2 and 3. In particular, the limiting values of C are nearly the same. To understand the origin of this limiting value in mathematical terms we have attempted a general solution for arbitrary

mode number using a Taylor series expansion for m_j and $\delta\mu_j$ truncated to two terms (next).

e. Asymptotic analysis

The Taylor series

$$m_j = 1 - \mu_j^2 + U \left[1 - \frac{1}{2} \mu_j^2 - \frac{1}{8} \mu_j^4 + O(\mu_j^6) \right] \tag{2.40a}$$

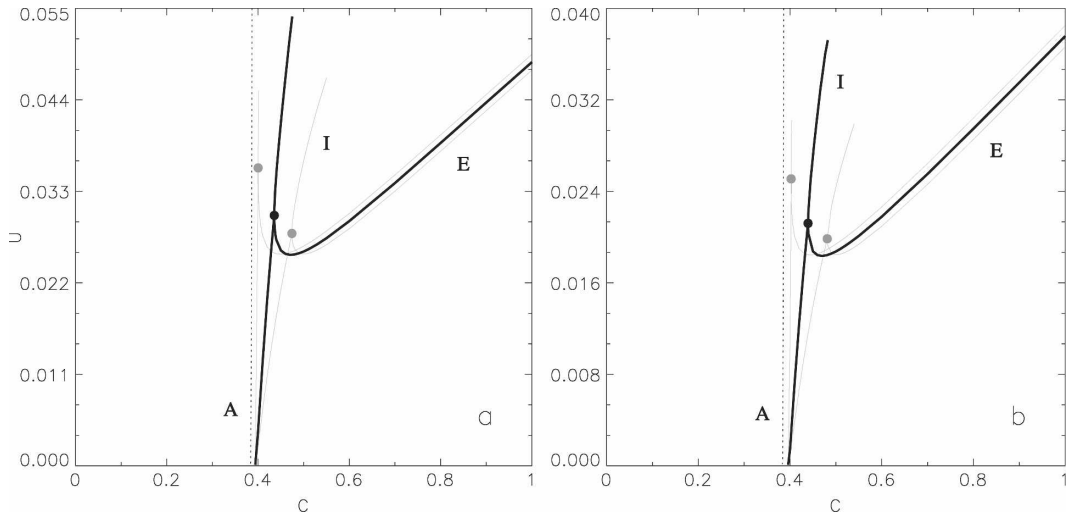


FIG. 9. Same as in Fig. 8, but for (a) mode 4 and (b) mode 5. For comparison, the lower part of the interior solution for mode 2 with $p = 1/4$ is also shown (dotted line).

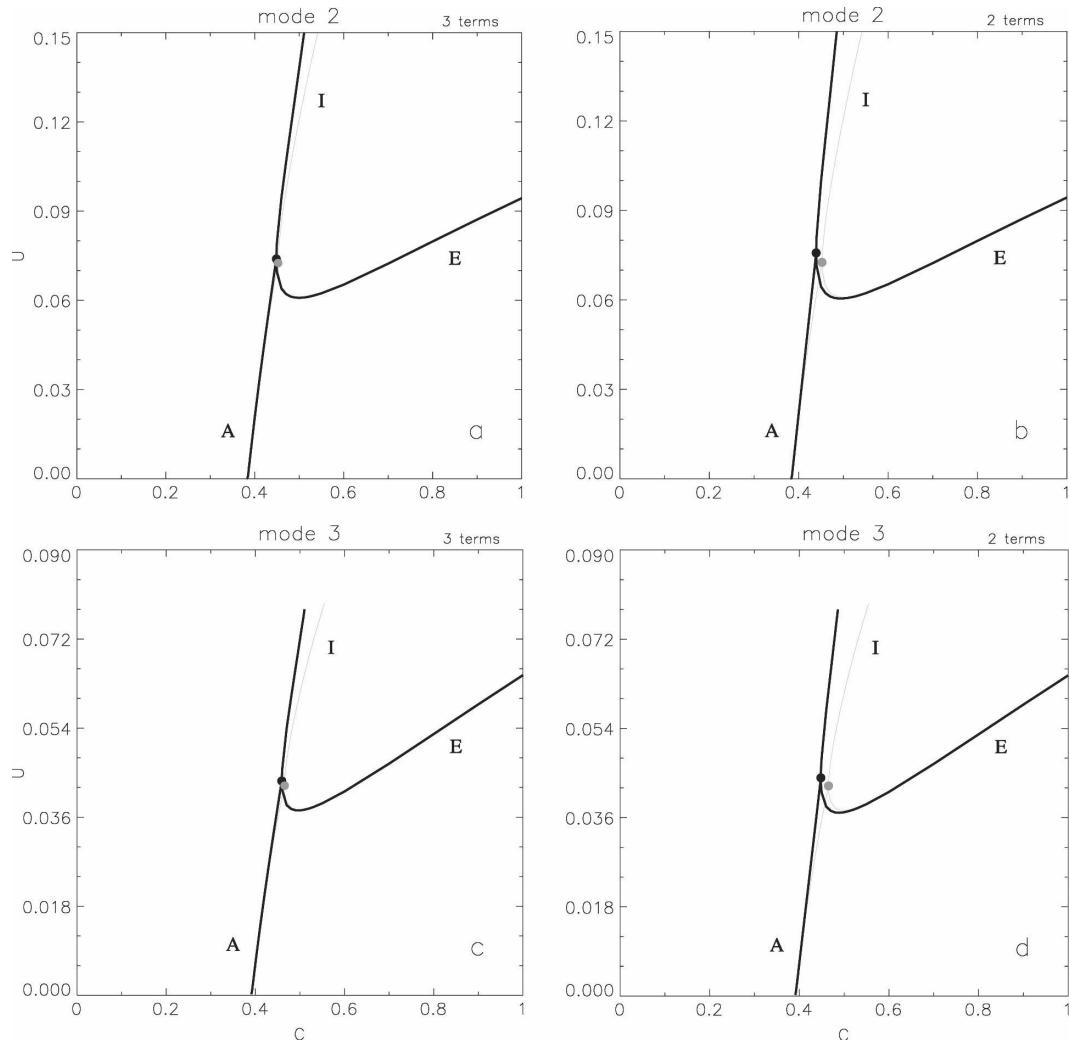


FIG. 10. Taylor series approximations (thick line) to exact solutions (thin line) for (a), (b) mode 2 and (c), (d) mode 3 with $p = 1/4$.

$$\delta\mu_j = \frac{\sqrt{U}}{C} \left[1 \pm \frac{1}{4} \mu_j^2 + \frac{5}{32} \mu_j^4 + O(\mu_j^6) \right] \quad (2.40b)$$

are useful in many cases of interest ($p = \pm 1/4$ in 2.40b). These expansions are quite good for most μ_j but fail miserably as $|\mu_j| \rightarrow 1$ and therefore should be used with caution. The results shown above were based on exact formulas; nevertheless, the accuracy of the truncated expansion will be apparent for all μ_j in the examples shown.

Approximate results obtained by truncating the Taylor series expansion to its leading two or three terms are shown in Figs. 10a,b for modes 2 and 3, respectively, with $p = 1/4$. As anticipated from Figs. 4 and 5, the three-term truncation is accurate over most of the range, thanks to the absence of jets near the pole,

where the Taylor series fail. This is partly a consequence of the construction of the theoretical model, wherein μ_p is determined by the global angular momentum constraint; that is, it does not depend explicitly on the Rhines scale, which is undefined at the outer edges of the staircase (where $\bar{u} = 0$) or poles (where $\beta = 0$). The two-term truncation is less accurate, but it should be noted that this level of approximation enables a perturbation solution for μ_p and μ_p^3 (see below). We expect the perturbation method to be useful in alternative models of the PV staircase that incorporate more sophisticated principles of GFD into the model constraints (e.g., a flux parameterization for Rossby waves).

When the Taylor series are truncated to two terms, a perturbation method may be used to understand asymptotic properties of the solution near the limiting

value of C . For even modes (with their first step beginning at the equator) the hemisphere-integrated angular

momentum may be divided into an interior staircase part and a ‘‘polar’’ part:

$$\begin{aligned} & \sum_{j=0}^{N-1} \frac{1}{2} (m_j + m_{j+1}) \frac{1}{2} (\delta\mu_j + \delta\mu_{j+1}) + \frac{1}{2} (m_N + m_p) (\mu_p - \mu_N) \\ &= \sum_{j=0}^{N-1} \left[(1 + U) - \left(1 + \frac{1}{2} U \right) \hat{\mu}_j^2 \right] \frac{\sqrt{U}}{C} \left(1 + \frac{1}{4} \hat{\mu}_j^2 \right) + \frac{1}{2} \left[1 - \mu_N^2 + U \left(1 - \frac{1}{2} \mu_N^2 \right) + 1 - \mu_p^2 \right] (\mu_p - \mu_N) \\ &= (1 + U) \frac{\sqrt{U}}{C} \sum_{j=0}^{N-1} (1 + a_2 \hat{\mu}_j^2) + \left[1 - \hat{\mu}_N^2 + \frac{1}{2} U \left(1 - \frac{1}{2} \mu_N^2 \right) \right] (\mu_p - \mu_N), \end{aligned} \tag{2.41}$$

where

$$\hat{\mu}_j^2 = \frac{1}{2} (\mu_j^2 + \mu_{j+1}^2) \tag{2.42a}$$

$$a_2 = \frac{1}{4} - \frac{1 + U/2}{1 + U}. \tag{2.42b}$$

The subscript on a_2 designates a coefficient for the second term of the expansion, although it is a nonlinear function of the auxiliary variable U . This dependence is ultimately relegated to a higher order in μ_j because the coefficient a_2 is multiplied by μ_j^2 , while its own variation is $O(\mu_j^2)$. When the lowest-order value $a_2 = -3/4$ is then substituted into (2.41), and we make use of the relation

$$U = C^2 \delta\mu_0^2, \tag{2.43}$$

the angular momentum constraint becomes

$$\begin{aligned} \delta\mu_0 \sum_{j=0}^{N-1} \left(1 + C^2 \delta\mu_0^2 - \frac{3}{4} \hat{\mu}_j^2 \right) \\ + \left(1 - \hat{\mu}_N^2 + \frac{1}{2} C^2 \delta\mu_0^2 \right) (\mu_p - \mu_N) = \mu_p - \frac{1}{3} \mu_p^3. \end{aligned} \tag{2.44}$$

Viewing this equation as a perturbation expansion in μ_p truncated to the leading two terms (of odd order only) and equating its first- and third-order parts gives

$$\delta\mu_0 N + [\mu_p - \mu_N^{(0)}] = \mu_p \tag{2.45a}$$

$$\begin{aligned} \left(C^2 N - \frac{3}{4} S_2 \right) \delta\mu_0^3 + \frac{1}{2} [(C^2 - N^2) \delta\mu_0^2 - \mu_p^2] \\ \times [\mu_p - \mu_N^{(0)}] - \mu_N^{(2)} \delta\mu_0^2 = -\frac{1}{3} \mu_p^3, \end{aligned} \tag{2.45b}$$

where

$$\mu_N = \mu_N^{(0)} + \mu_N^{(2)} \delta\mu_0^2 + O(\mu_j^5) \tag{2.46a}$$

$$S_2 = \sum_{j=0}^{N-1} \left(j^2 + j + \frac{1}{2} \right) = \frac{N}{6} (2N^2 + 1) \tag{2.46b}$$

so that

$$\mu_N^{(0)} = N \delta\mu_0 \tag{2.47a}$$

$$\begin{aligned} (C^2 N - S_2) \delta\mu_0^3 + \frac{1}{2} [(C^2 - N^2) \delta\mu_0^2 - \mu_p^2] (\mu_p - N \delta\mu_0) \\ = -\frac{1}{3} \mu_p^3. \end{aligned} \tag{2.47b}$$

The former equation suggests that $\mu_j^{(0)} = j \delta\mu_0$ so that variations of jet spacing caused by the β dependence of the Rhines scale may be neglected at first order. These variations are properly accounted for at third order both (i) within the staircase [first term on the lhs of (2.44)] and (ii) in the outer rhomboid [second term of the lhs of (2.44)] provided that a small correction to μ_N is retained, which may be evaluated noting that

$$\begin{aligned} \mu_N = \sum_{j=0}^{N-1} \frac{1}{2} (\delta\mu_j + \delta\mu_{j+1}) = \frac{\sqrt{U}}{C} \sum_{j=0}^{N-1} \left(1 + \frac{1}{4} \hat{\mu}_j^2 \right) \\ = N \delta\mu_0 + \frac{1}{4} S_2 \delta\mu_0^3. \end{aligned} \tag{2.48}$$

The first term on the rhs of (2.48) agrees with (2.47a) and in (2.47b) was substituted for the $\mu_N^{(0)}$ in (2.45b); the second term was likewise substituted for $\mu_N^{(2)}$ and subsequently absorbed into the first term on the lhs of (2.47b). When $p = 1/4$, the Rhines scale increases slowly in the sine of latitude, causing μ_N to slightly exceed its lowest-order value predicted by equal spacing in μ . Exactly the opposite occurs when $p = -1/4$ so that μ_N is slightly less than its lowest-order value. If exactly equal spacing in μ is assumed a priori ($p = 0$), (2.47a) becomes exact ($\mu_N \equiv N \delta\mu_0$) and $\mu_N^{(2)}$ disappears, while the factor 3/4 on the lhs of (2.45b) reverts to unity; fortuitously, these two changes cancel.

Equation (2.47b) may be differentiated with respect to $\delta\mu_0$, then setting $\partial\mu_p/\partial\delta\mu_0 = 0$ to match the situation in the lower branch of the interior solution (namely, to maximize μ_p with respect to U holding C fixed, equivalent to a variation of μ_p with respect to $\delta\mu_0$, holding C fixed) to give

$$3\delta\mu_0^2(C^2N - S_2) + [(C^2 - N^2)\delta\mu_0](\mu_p - N\delta\mu_0) + \frac{1}{2}[(C^2 - N^2)\delta\mu_0^2 - \mu_p^2](-N) = 0. \quad (2.49)$$

Equations (2.47b) and (2.49) may be written as

$$A + B(x - N) + \frac{1}{3}x^3 = 0 \quad (2.50a)$$

$$3A + (2B + x^2)(x - N) - BN = 0, \quad (2.50b)$$

where

$$x = \frac{\mu_p}{\delta\mu_0} \quad (2.51a)$$

$$A = C^2N - S_2 \quad (2.51b)$$

$$B = \frac{1}{2}(C^2 - N^2 - x^2) \quad (2.51c)$$

from which it is easy to show that $B = -xN$ whereupon $C = x - N$. This simple relation was validated in our examples near the limiting value of C . Further manipulation shows that x is a solution of

$$x^2 = 3N^2 + \frac{N}{2x}(1 - 4N^2). \quad (2.52)$$

As it turns out, x increases almost linearly in N , so the difference $C = N - x$ is remarkably steady, $C \approx 0.4$, in the range $N = 1 - 20$ as shown in Fig. 11. In the limit of large N , (2.52) predicts that $C \rightarrow 1/\sqrt{6} \approx .408$. Recalling that C is like an inverse spatial scale in (2.34), large N implies a geometrical Rhines-scale factor for the sphere (i.e., the ratio of jet spacing to the Rhines scale associated with the jet velocity) equal to $\sqrt{6}$. The asymptotic values shown in Fig. 11 agree with the limiting values of C shown in our earlier examples to within 1%–2%. This statement also applies to solution trajectories for modes higher than 5 (not shown here).

The corresponding analysis of odd modes, with a half stair step beginning at the equator, proceeds along similar lines and yields similar values of C , also shown in Fig. 11. If one were to substitute a continuous curve for the discrete values shown, the curve for odd modes is exactly that of even modes but shifted to the right by 1/2. By calling out the first term in the summation of (2.41), noting that

$$m_0 = m_1 \quad (2.53a)$$

$$\mu_1 = \frac{1}{2} \delta\mu_1, \quad (2.53b)$$

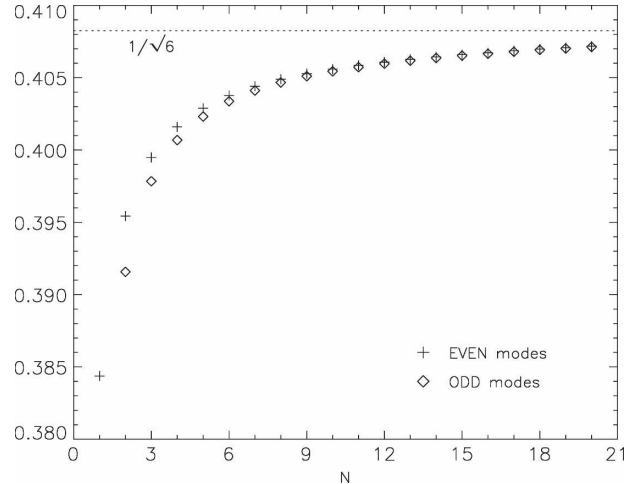


FIG. 11. Asymptotic values of C for even and odd modes, as a function of N .

equations analogous to (2.47a) and (2.47b) are obtained as follows:

$$\mu_N^{(0)} = \hat{N}\delta\mu_0 \quad (2.54a)$$

$$(C^2\hat{N} - \hat{S}_2)\delta\mu_0^3 + \frac{1}{2}[(C^2 - \hat{N}^2)\delta\mu_0^2 - \mu_p^2](\mu_p - \hat{N}\delta\mu_0) = -\frac{1}{3}\mu_p^3, \quad (2.54b)$$

where

$$\hat{N} = N - \frac{1}{2} \quad (2.55a)$$

$$\hat{S}_2 = \frac{1}{8} + \sum_{j=1}^{N-1} \left(j^2 + \frac{1}{4} \right) = \frac{1}{4}\hat{N} + \frac{1}{3} \left(\hat{N}^2 - \frac{1}{4} \right) \hat{N}. \quad (2.55b)$$

Once again a small correction to μ_N is retained:

$$\begin{aligned} \mu_N &= \frac{1}{2} \delta\mu_1 + \sum_{j=1}^{N-1} \frac{1}{2} (\delta\mu_j + \delta\mu_{j+1}) \\ &= \frac{1}{2} \delta\mu_1 + \frac{\sqrt{U}}{C} \sum_{j=1}^{N-1} \left(1 + \frac{1}{4} \hat{\mu}_j^2 \right) \\ &= \frac{1}{2} \delta\mu_0 \left(1 + \frac{1}{4} \mu_1^2 \right) + (N-1)\delta\mu_0 \\ &\quad + \frac{1}{4} \delta\mu_0^3 \sum_{j=1}^{N-1} \left(j^2 + \frac{1}{4} \right) \\ &= \hat{N}\delta\mu_0 + \frac{1}{4} \delta\mu_0^3 \hat{S}_2. \end{aligned} \quad (2.56)$$

From this point the equations are isomorphic to those of even modes but with \hat{N} and \hat{S}_2 substituted for N and S_2 . Therefore $C = x - \hat{N}$, and the asymptotic value of C at large N is the same. In fact, the entire curve is the same (shifted by 1/2) because a relation isomorphic to (2.52) is obtained for odd modes as well, and (2.55b) yields the same sum as (2.46b), but with \hat{N} in place of N . This equivalence of even and odd modes suggests that both could be analyzed with identical formulas in an alternative model using half stair steps instead of full steps.

When the (prograde) westerly jets of the staircase are assumed to have equal amplitude, the strength of (retrograde) easterly jets generally varies in latitude in order to accommodate (i) the variation of the moment arm, proportional to $\sqrt{1 - \mu^2}$, and (ii) the variation (if any) of spacing between the westerly jets. For a given deviation of m from the resting parabola, a smaller moment arm approaching the poles requires stronger easterlies; the same is true for larger jet spacings, which imply a larger deviation of m . In our first case ($p = 1/4$) using the variable Rhines scale (2.34), both factors play an approximately equal role. To see this, note that the deviation from the resting parabola is

$$\Delta m = m_j + \frac{m_{j+1} - m_j}{\mu_{j+1} - \mu_j} (\mu - \mu_j) - (1 - \mu^2) \tag{2.57a}$$

$$\frac{\partial \Delta m}{\partial \mu} = \frac{m_{j+1} - m_j}{\mu_{j+1} - \mu_j} + 2\mu = 0 \quad \text{at} \quad \mu = \mu_m, \tag{2.57b}$$

whereupon to $O(\mu_j^4)$,

$$\mu_m = \frac{1}{2} (\mu_j + \mu_{j+1}) \tag{2.58a}$$

$$m_m = 1 + U - \hat{\mu}_j^2 \tag{2.58b}$$

$$\begin{aligned} \Delta m_m &= U + \mu_m^2 - \hat{\mu}_j^2 \\ &= U - \frac{1}{4} (\mu_{j+1} - \mu_j)^2 \end{aligned} \tag{2.59}$$

or

$$\Delta(m_e - m_m) \propto (\delta\mu_j + \delta\mu_{j+1})^2. \tag{2.60}$$

Another way to look at this is to note that the deviation is simply the difference between a straight line and a parabola, which can always be written as a μ translation of the original parabola; that is, the deviation itself is a parabola. With $p = 1/4$ in (2.34) the maximum deviation of m below the resting parabola varies as $(1 - \mu^2)^{-1/2}$. The maximum deviation of \bar{u} contains an addi-

tional factor of $(1 - \mu^2)^{-1/2}$ from the moment arm, bringing the total variation to $(1 - \mu^2)$ as shown in Fig. 12a. For constant jet spacing in μ ($p = 0$) the variation is from the moment arm only (Fig. 12c). With $p = -1/4$ in (2.34) the Rhines scaling is reversed in the μ coordinate, bringing the (prograde) westerly jets closer together, approaching the poles. (It should be kept in mind that their spacing still *increases* approaching the pole when viewed in the θ coordinate, as in the other two cases.) In this case the (retrograde) easterly jets are equal (Fig. 12e). The theory outlined above evidently applies to a more general class of jet strength/spacing relationships, although we have yet to explore the function space in detail. The corresponding plots of m deviation are shown in Figs. 12b,d,f. From the first two of these panels it is apparent that some transfer of prograde (westerly) angular momentum to the equator is required, slowly varying in μ , even for solutions such as those lying on the upper end of the asymptotic branch near the coalescence point.

The specification that μ_p be the maximum possible for a given value of C is based loosely in the notion that small-scale forcing of the (nearly barotropic) model applied uniformly on the sphere will tend to create a PV staircase extending into polar latitudes (Scott and Polvani 2007).⁴ The preceding analysis made this assumption, but additional insight can be obtained from an alternative condition that the outer segment be tangent to the resting parabola, as discussed in connection with mode 1 in the previous subsection. This condition automatically excludes easterlies adjacent to μ_p , whether large or small. The majority of nearly barotropic cases shown by Scott and Polvani, in fact, have polar westerlies, although the polar jet is usually not sharp and its maximum is somewhat weaker than the jets of the staircase. In the analytical model such a situation is found in the interior solution above the coalescence point (when constrained to maximize μ_p , as above) or when tangency at μ_p is imposed as an alternative.

Values of C and U at the coalescence point are shown in Fig. 13, using the jet spacing (2.34) with three values of p . Coalescence values of C increase slowly with mode number while U drops precipitously, approximately as $n^{-1.8}$ over the range shown, relevant to known planetary atmospheres. The exponent is reasonably close to 2, consistent with our earlier notion that the deviation of m from the resting parabola is proportional to jet spacing squared, with jet spacing approximately in-

⁴ The angular momentum constraint applies to freely decaying turbulence and, in our case, to a forced system in which the random small-scale forcing imparts no angular momentum to the globally averaged flow.

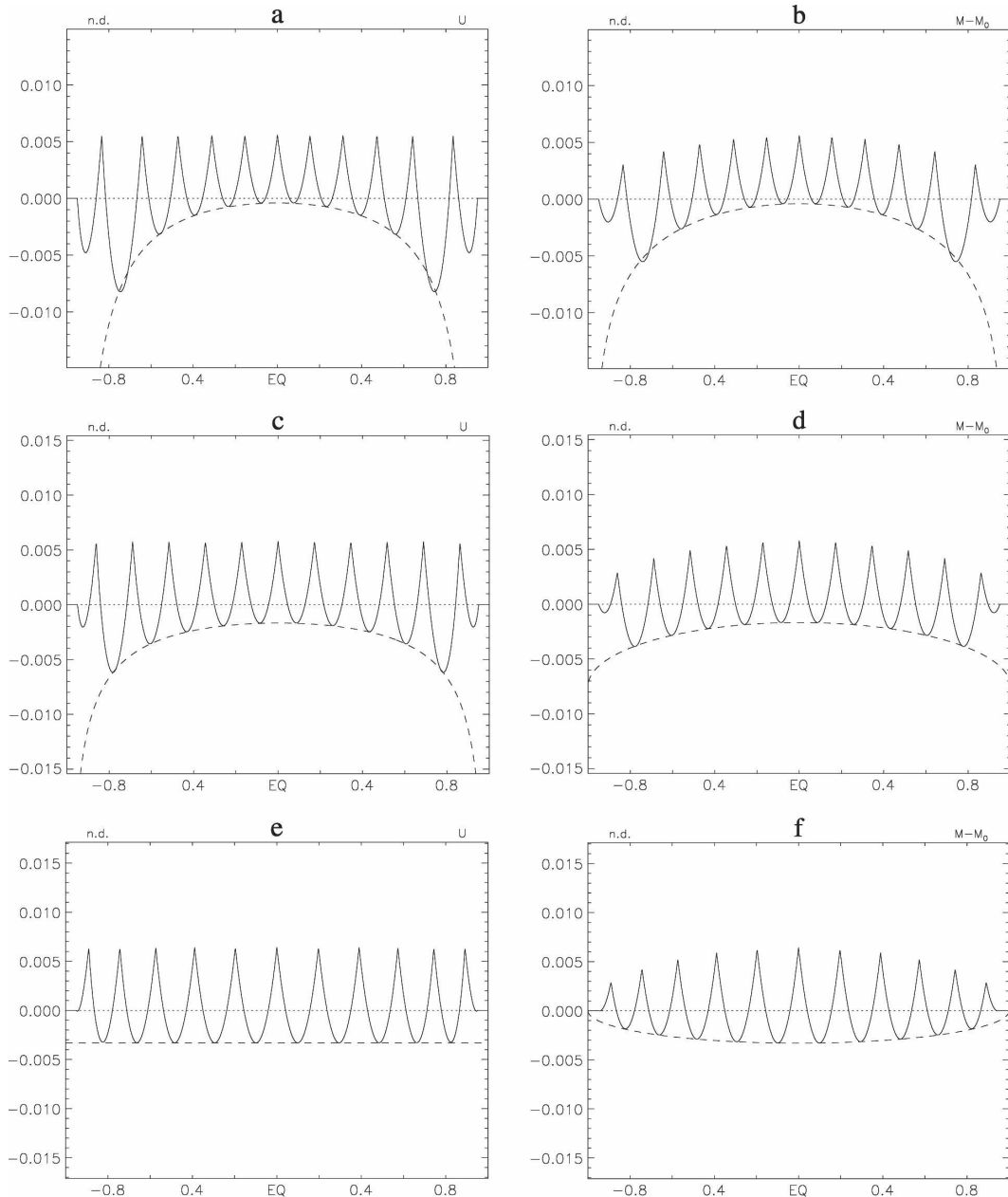


FIG. 12. Illustration of mode 10 solutions all having $\mu_p = 0.95$, for (a), (b) $p = 1/4$, (c), (d) $p = 0$, and (e), (f) $p = -1/4$. Dashed curves show the different powers of $(1 - \mu^2)$ appropriate for each of the cases.

versely proportional to mode number. Coalescence values of U in the three cases are nearly identical at large N , since the formula for jet spacing becomes irrelevant when the number of jets is large. When $p = -1/4$ the coalescence and limiting values of C are almost identical, thanks to the steep vertical slope of the left solution branch. This is a convenient result because one may then use asymptotic values (representing solutions trapped near the equator) as a good estimate for other

solutions near the coalescence point than span the globe.

A final observation is that if the number of jets varies approximately as the inverse square root of U , it therefore varies approximately as the inverse one-fourth power of zonal kinetic energy. In a model configuration with energy increasing linearly with time owing to a constant input of energy at small scales, the temporal decrease in the *number* of jets is expected to be very

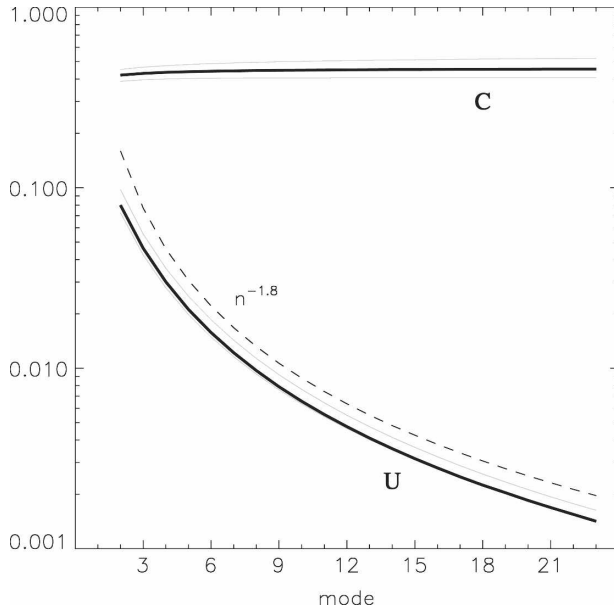


FIG. 13. Coalescence values of C and U as a function of mode number n . The thick curves are for $p = 0$. In accord with Fig. 8, values of C (U) for $p = -1/4$ are slightly below (above) the values of $p = 0$ (thin curves). The reverse applies to $p = 1/4$ although values of U are nearly the same. The dashed curve shows an approximate power-law fit to U as a function of mode number n .

slow. Indeed, it proves difficult to examine steady-state behavior in such a configuration because the required integration time is very long.

3. Numerical results

The simplest system in which to study the effects of potential vorticity mixing and angular momentum conservation is that of a single layer of fluid of uniform depth on the sphere. This system is governed by the barotropic vorticity equation:

$$\zeta_t + J(\psi, \zeta_a) = 0, \tag{3.1}$$

where $\zeta = \Delta\psi$ is the vorticity, ψ is streamfunction, and the absolute vorticity $\zeta_a = \zeta + f$, which, as in section 2, is here the same as the potential vorticity.

a. Numerical procedure

We solve (3.1) numerically using a pseudospectral model with a horizontal truncation of T170 spherical harmonics and time stepping with a semi-implicit leap-frog scheme. The numerical model is the same as described in Scott and Polvani (2007) but adapted to solve the barotropic vorticity equation only.

The system is forced and dissipated by the inclusion of additional terms on the rhs of (3.1). In particular, F

is a random process, δ correlated in time, designed to input energy at a constant rate ϵ_0 in a range of spherical harmonics centered on $n_f = 42$. The term D_ζ is made up of scale-selective diffusive operators acting at small and large scales: hyperdiffusion to arrest the enstrophy cascade before the truncation scale; and hypodiffusion to remove energy at large scales and allow equilibration of the large-scale flow. We note that the form of the hypodiffusion (an inverse Laplacian) is equivalent to a damping on the streamfunction, and therefore can be considered as a crude approximation to the more physically relevant radiative cooling in more sophisticated equivalent barotropic or shallow-water systems. These terms take the same form as the terms F and D_ζ in Scott and Polvani [2007; see in particular Eqs. (9a), (11), and (15), therein].

We present results from calculations in which energy is injected at a constant rate ϵ_0 . Two sets of experiments are performed, with $\epsilon_0 = 10^{-6}$ and $\epsilon_0 = 10^{-7}$, in units of $a^2(\Omega/2\pi)^{-3}$. The model is integrated until time $t = T$, where $T = 10^4 \times (2\pi/\Omega)$ for the case $\epsilon_0 = 10^{-6}$ and $T = 2 \times 10^4 \times (2\pi/\Omega)$ for the case $\epsilon_0 = 10^{-7}$, that is, $T = 10^4$ and $T = 2 \times 10^4$ planetary rotations, respectively. This length of integration generally allows for a quasi-equilibrated state to be reached, although in some cases complete equilibration requires more time. For comparison with the analysis of section 2, in the following discussion all quantities are scaled on a and Ω unless otherwise noted. For each energy injection rate, an ensemble of calculations is performed comprising 30 realizations of the forcing. As will be described, considerable variability in mode number exists for different realizations under otherwise identical parameter values.

b. Mode selection

We first consider the case $\epsilon_0 = 10^{-6}$. For this ensemble, the equilibrium solutions fall roughly into three groups: prograde equatorial flow, retrograde equatorial flow, or mixed, the latter consisting typically of hemispherically asymmetric states. Of these three groups we consider only the former two. In a three-dimensional system, asymmetric states with nonzero cross-equatorial shear would tend to be inertially unstable and would in general not be observed: here they can be considered as an artifact of the single-layer system that has no means to prevent angular momentum maximizing away from the equator (see section 4a). We define prograde cases as those whose value of \bar{u} at the equator exceeds one-half of the global maximum \bar{u} , and retrograde cases as those whose value of \bar{u} at the equator is less than one-half of the global minimum \bar{u} . By this definition, of the 30 ensemble members, 9 are prograde

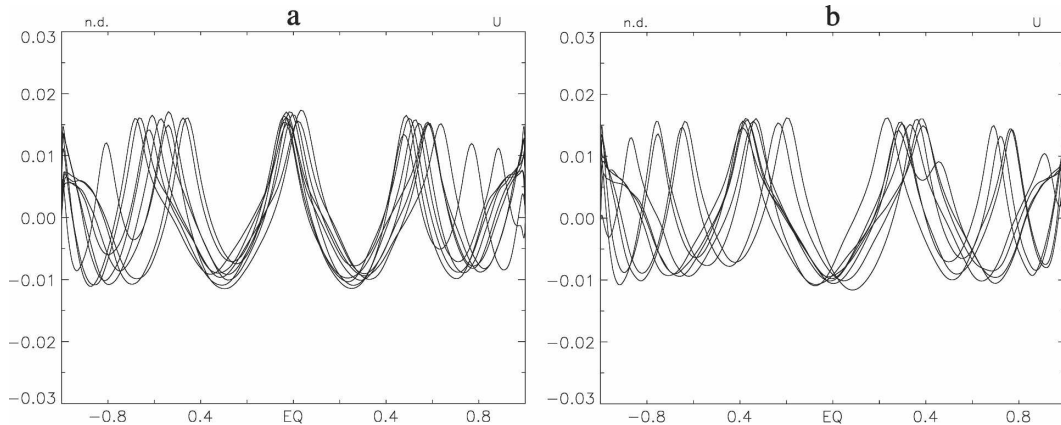


FIG. 14. Equilibrium \bar{u} from an ensemble calculation of 30 realizations with $\epsilon = 10^{-6}$. (a) Nine prograde equatorial flows are shown, representing all cases for which $\bar{u}(\mu = 0) \geq 1/2 \max_{\mu}(\bar{u})$; (b) eight retrograde flows show all cases for which $\bar{u}(\mu = 0) \leq 1/2 \min_{\mu}(\bar{u})$.

and 8 are retrograde. The steady-state zonal velocity \bar{u} at $t = 10^4$ for the two groups is shown in Fig. 14. With respect to the axisymmetric solutions, the prograde cases here correspond to mode 4 solutions (three jets per hemisphere), while the retrograde cases correspond to either mode 3 or mode 5 solutions (two or three jets per hemisphere; in each case the polar westerlies are counted as jets).

The approximately equal occurrence of prograde and retrograde solutions stands in contrast to the situation of freely decaying barotropic turbulence, where retrograde equatorial jets have been more frequently documented. Ensemble calculations of freely decaying barotropic and shallow-water turbulence, starting from different initial conditions, indicate that prograde jets can form in certain parameter regimes, but that retrograde jets are generally preferred (Kitamura and Ishioka 2007). In forced-dissipative shallow-water turbulence, Scott and Polvani (2007) observed a tendency toward retrograde equatorial jets with decreasing deformation radius. In the forced-dissipative barotropic system, on the other hand, Huang and Robinson (1998) observed both prograde and retrograde equatorial jets depending on the level of forcing. Large ensemble calculations of the forced-dissipative barotropic system appear not to have been previously documented; Fig. 14 indicates that both prograde and retrograde are approximately equally realizable in this system.

The magnitudes of the jets in Fig. 14 are almost 0.02, roughly half of the values obtained for the limiting solutions of the axisymmetric model (e.g., Figs. 5 and 7 give a value of around 0.04 for mode 3). As will be seen next, the eddy mixing of PV is incomplete in the full model. Note that in each group in Fig. 14 the maximum jet speeds are similar. This is consistent with Fig. 7 and

the corresponding case for mode 4 (not shown) in that there is an overlap of the ranges of U for which the upper branches ($\mu_p = 1$) occur. The asymmetric solutions (which comprise less than half of the total ensemble, and which will not be considered here) can be regarded as containing different mode numbers in different hemispheres, a situation that is not precluded by the analysis of section 2.

A similar pattern is found in the weakly forced ensemble with $\epsilon_0 = 10^{-7}$ (not shown). The range of possible solution states appears to increase, presumably because more mode numbers can coexist for the same maximum jet strength. Of the 30 members of the ensemble, 5 are prograde and 8 are retrograde, by the above definitions. Jet strengths reach around 0.007, and the typical mode numbers are between 5 and 7.

During the time evolution toward equilibrium both prograde and retrograde cases emerge out of similar early time evolution: significant differences in jet structure develop slowly in time. Often, cases that are retrograde at early times develop a prograde equatorial jet through the merger of the two jets straddling the equator; in other cases an equatorial jet will drift off the equator to be replaced by easterlies.

The process of jet merger may be considered in terms of the axisymmetric solutions described in section 2: when the jet strength is small, the angular momentum constraint implies that jet spacing in the piecewise linear solution must be correspondingly small. As the jet strength increases, jet spacing must also increase. Jet mergers can therefore be considered as a transition from a state where a higher mode number exists but subsequently becomes unrealizable within a barotropically stable flow. Although the axisymmetric solution must be regarded as a limiting case, a similar PV and

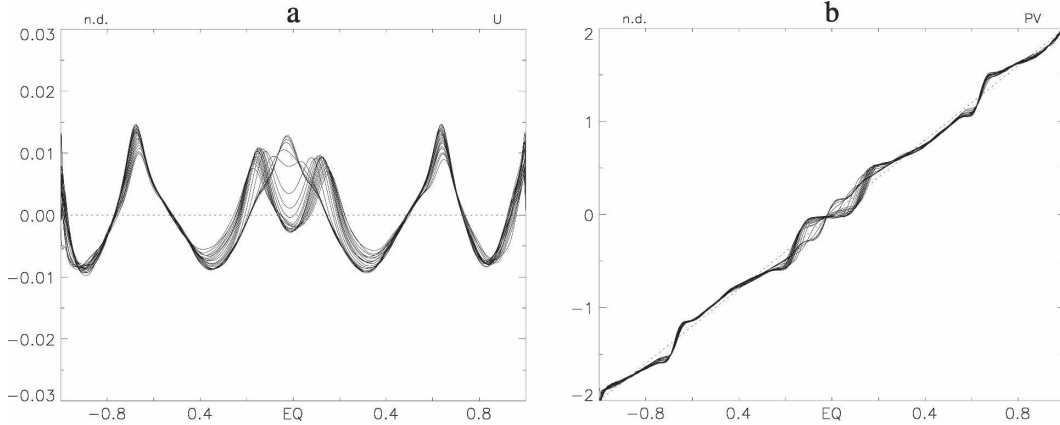


FIG. 15. Time evolution of (a) zonal-mean zonal velocity \bar{u} and (b) potential vorticity ζ_a during an equatorial jet merger. Lines are drawn at times $t = \{200, 220, 240, \dots, 600\} \times 2\pi$.

angular momentum structure exists in the full model, consistent with the hypothesis that eddy mixing generally leads to an angular momentum-conserving rearrangement of the PV. In the full model, PV mixing between the jets is incomplete, giving rise to sloping steps. Similarly, the risers are not vertical but sloping, partly due to the zonal averaging of a PV jump that is not perfectly zonally aligned (but slightly wavy), and partly due to the fact that the jump itself is not perfect owing to the presence of diffusion in the model.

An example is given in Fig. 15, which shows the merger of two jets straddling the equator into a single equatorial jet. At early times the subtropical jets are accelerating, because of the constant input of energy by the forcing and the accumulation in the zonal flow. At the earliest times shown, the PV gradients across the equator are positive, corresponding to a barotropically stable configuration. As time increases, mixing across the equator becomes progressively more complete, eventually reaching the marginally stable situation of zero PV gradient. At this point jet merger occurs. In terms of Fig. 6, the evolution corresponds to moving upward along the upper branch as U increases. When the higher-mode solution is no longer realizable within a barotropically stable configuration, a catastrophic change in the flow structure occurs toward a lower-mode solution, realizable at larger U .

c. Zonal momentum balance

We next describe the momentum balance during the adjustment of the flow to equilibrium, and how eddy fluxes organize an acceleration of the zonal mean flow. By (2.15a), the zonal mean flow acceleration is associated with an eddy-induced flux of potential vorticity. In particular, any jet acceleration must be accompanied by an upgradient flux of potential vorticity.

First, we illustrate the identity during the evolution toward equilibrium. Figure 16 shows the zonal mean flow \bar{u} , the acceleration $\partial\bar{u}/\partial t$, and the eddy-induced PV flux $\overline{v'\zeta'}$ at the time of the jet merger in Fig. 15. The two subtropical jets are decelerating and the equatorial jet is accelerating. The acceleration is seen to correspond closely with the eddy fluxes as expected.

Although less dramatic, the midlatitude jets are also accelerating at this time. Again $\partial\bar{u}/\partial t$ is correlated with $\overline{v'\zeta'}$, but now greater (relative) departures can be seen, mostly due to small-scale structure in the latter. Differences between $\overline{v'\zeta'}$ and $\partial\bar{u}/\partial t$ can arise only through the effects of dissipation; since the forcing is δ correlated in time, the contribution to $\overline{v'\zeta'}$ (which is averaged in time over intervals $\Delta t = 10$) is negligible. Furthermore, small-scale structure in $\partial\bar{u}/\partial t - \overline{v'\zeta'}$ can be balanced

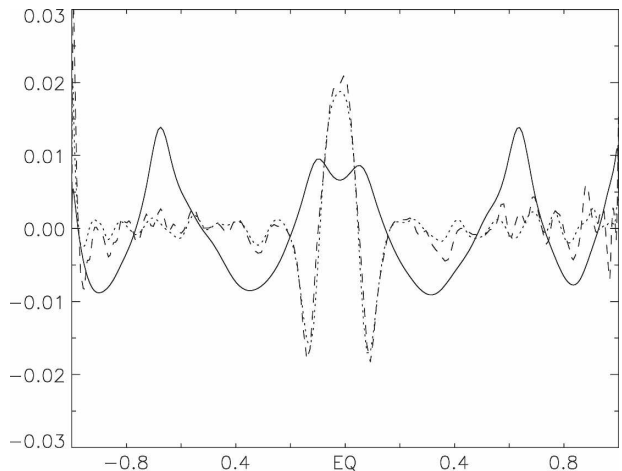


FIG. 16. Zonal-mean velocity \bar{u} (solid), acceleration $\partial\bar{u}/\partial t$ (dotted; $\times 5000$), and eddy PV flux $\overline{v'\zeta'}$ (dashed; $\times 5000$) at the time of jet merger ($t = 500 \times 2\pi$) shown in Fig. 15.

only by the hyperdiffusion, since hypodiffusion is only effective at the largest scales.

The small-scale structure in $\overline{v'\zeta'}$ can best be examined at equilibrium when $\partial\bar{u}/\partial t \sim 0$. Figure 17 shows in more detail the correspondence of (quasi) equilibrium $\overline{v'\zeta'}$ both with the jet maxima and with the PV profile. A surprising feature is that $\overline{v'\zeta'}$ appears to maximize at the jet maxima. This region is associated with a sharp PV gradient, which in some sense can be considered as a barrier to eddy mixing, and which therefore might be expected to coincide with a *minimum* in $\overline{v'\zeta'}$. On the other hand, since the PV gradients are concentrated at the jet, this region is also where wave activity is concentrated. In the limit of a perfect staircase, nonzero PV gradients only exist at the jet maximum, and consequently eddy fluxes must necessarily be confined there. Maxima of $\overline{v'\zeta'}$ aligned with the jet core were also found in Huang and Robinson (1998) during the acceleration phases of the jet. At the higher resolution used here, the finer structure of the eddy fluxes within the jet region becomes clear. Note, for example, the regions of weak $\overline{v'\zeta'}$ on either side of the maxima, which correspond closely to the narrow regions of almost zero PV gradients on either side of the PV riser, again consistent with the observation that eddy fluxes must be confined to regions of nonzero PV gradient.

d. Jet spacing

We close this discussion with a consideration of the statistics of jet spacing and strength across multiple realizations of the forcing. Although roughly similar jet numbers and spacing emerge for a given forcing amplitude (since this determines the energy and hence ap-

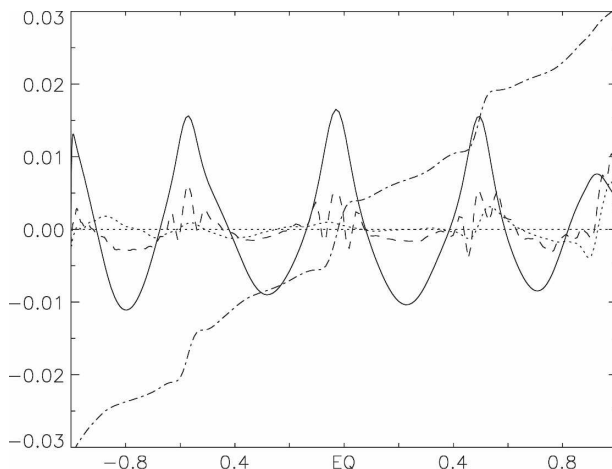


FIG. 17. Zonal-mean velocity \bar{u} (solid), acceleration $\partial\bar{u}/\partial t$ (dotted; $\times 10\,000$), eddy PV flux $\overline{v'\zeta'}$ (dashed; $\times 10\,000$), and zonal mean PV $\bar{\zeta}_a$ (dashed-dotted; $\times 0.01$) at quasi equilibrium (averaged over the last fifth of the integration).

proximate zonal wind speed of the jets), as discussed above variations do exist and different mode numbers are obtainable under identical physical conditions.

Recall that in section 2, three different models were discussed relating spacing to jet strength, namely, $\delta\mu = C^{-1}(1 - \mu^2)^{-1/4}\sqrt{U}$ (stretched Rhines scaling in μ), $\delta\mu = C^{-1}\sqrt{U}$ (uniform jet spacing in μ), and $\delta\mu = C^{-1}(1 - \mu^2)^{1/4}\sqrt{U}$ (compressed jet spacing in μ). The differences between these models was most apparent with regard to the strength of the interjet easterly flow and its μ dependence (Fig. 12). A casual inspection of many numerically generated equilibrated \bar{u} profiles (e.g., Fig. 14) immediately suggests that the latter model (compressed jet spacing in μ) is the most relevant. In the numerical simulations, easterlies are most often approximately constant in latitude; a small minority of cases has easterlies increasing toward the poles while the westerlies are relatively constant. We can make this more precise by considering the relationship between interjet easterlies to jet spacing occurring in all pairs of adjacent jets in the full set of both ensemble calculations. This provides equilibrium states ranging from mode 3 to around mode 7, which also contain large variability in jet spacing. Thus, for each pair of adjacent jets at μ_j and μ_{j+1} we define the spacing $\delta\mu_j = \mu_{j+1} - \mu_j$ and the magnitude of the interjet easterlies as $U_j = -\min_{\mu \in [\mu_j, \mu_{j+1}]} u(\mu)$.

Figure 18 shows the scatterplot of the $\delta\mu_j$ against

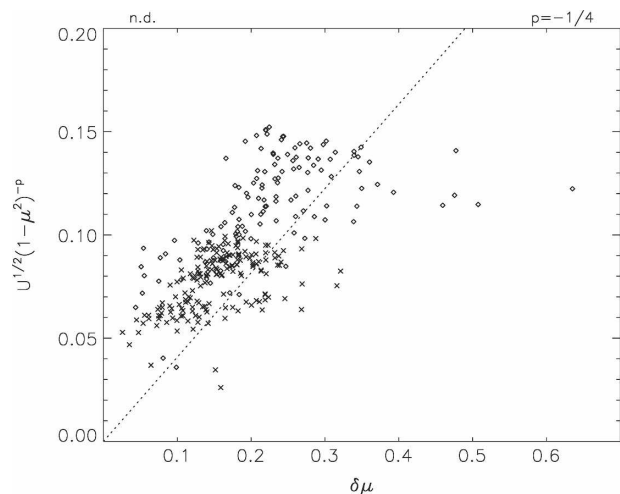


FIG. 18. Relation of jet spacing to jet strength, for $p = -1/4$. The idea is to determine which, if any, of the Rhines scalings in the range $-1/4 \leq p \leq 1/4$ best describe the numerical results. Of the three values illustrated in this paper, $p = -1/4$ displays the best fit, and the inferred slope of the fit is close to the asymptotic value of \sqrt{U}/C . Here, $\delta\mu$ is defined as the spacing between pairs of adjacent jets; U is defined as the minimum \bar{u} between the same pairs. Diamonds and crosses denote jet pairs from the ensembles with $\epsilon = 10^{-6}$ and $\epsilon = 10^{-7}$, respectively.

$(1 - \mu^2)^{-p} \sqrt{U}$ for $p = -1/4$. A compact relationship exists only for the case of compressed jet spacing in μ shown here. For the case of uniform jet spacing in μ ($p = 0$) all the U 's are approximately equal for a given realization, depending only on the total energy level (not shown). The dependence on μ is degenerate and no value of C is obtained. Similarly, no clear relation holds for the local Rhines scaling in μ ($p = 1/4$, not shown). For the compressed jet spacing, although there is considerable scatter, a value of $C \sim 0.4$ can be estimated from the slope of the best-fit line through the points. This value accords reasonably well with the asymptotic values of C derived in section 2e.

4. Two generalizations of the theoretical model

The numerical model of Scott and Polvani (2007), based on the shallow-water equations, admits a richer spectrum of jet behavior than the barotropic model. In particular, the wave activity and eddy fluxes become equatorially confined at small positive equivalent depth, so that westerly and easterly jets alike vary in amplitude with latitude, decreasing away from the equator. Although the model displays a statistical preference for symmetric states—namely, hemispheric symmetry of the PV staircase, whether even or odd— asymmetric states are sometimes obtained. In this section we suggest how the theoretical model may be generalized to handle such variations from the symmetric barotropic staircase.

a. Asymmetric solutions

It is tempting to dismiss hemispherically asymmetric PV staircases with cross-equatorial shear as irrelevant owing to equatorial inertial stability. Any process that moves the maximum m off the equator—thereby satisfying a necessary and sufficient condition for centrifugal inertial instability between the equator and m maximum—is countered by an inertial adjustment that tends to restore inertial stability. The notion, however, that inertial adjustment simply transports the maximum m back to the equator, restoring the initial (stable) profile of m , is incorrect. All that is required for inertial stability is a redistribution of m that flattens its gradient within and poleward of the unstable zone adjacent to the equator (Ortland and Dunkerton 2008, unpublished manuscript). As a result, asymmetric solutions are possible in the tropics. They are of course possible in dynamical models that do not admit inertial instability at all, for example, when the equivalent depth is larger than the marginal value for equatorial inertial instability. Such cases are included among those shown by Scott and Polvani (2007).

In the event that the hemispheres behave independently, the theoretical model described above may be applied to the hemispheres individually; there is no cross-equatorial transport of angular momentum or PV. Equatorial superrotation is of course excluded from such cases. Inertial adjustment may come into play in situations where some sort of cross-equatorial transport is attempted by the large-scale circulation, to be partially offset by the adjustment. It was argued by Dunkerton (1981), for example, that the diabatic circulation of the middle atmosphere attempts to create easterlies on the equator twice a year (the easterly phase of the semiannual oscillation) but that this advective process is partially countered and/or delayed by inertial adjustment (see, e.g., Hitchman and Leovy 1986, for evidence of the effect). One consequence of the adjustment is that the flow becomes barotropically unstable on the summer side of the equator. Barotropic instability is thought to be one of several possible mechanisms for excitation of the 2-day wave (Orsolini et al. 1997; Pendlebury and Dunkerton 2008, unpublished manuscript). It was suggested in section 2b that barotropic adjustment should be taken into account at the outer edges of the PV staircase. To be consistent with this reasoning we should therefore consider the combined effects of inertial and barotropic adjustment near the equator. As a practical matter—as long as the underlying dynamical model allows it—inertial instability is guaranteed to be effective in adjusting the flow to an inertially neutral state, whereas it is less certain that barotropic instability is equally effective in relaxing the flow to a barotropically neutral state. One of the cases shown by Scott and Polvani (2007), for example, displays a nonmonotonic final PV profile.

If the hemispheres are coupled and the coupling mechanisms include inertial and barotropic adjustment, the appropriate generalization of the analytical model is (i) to relax the requirement of hemispheric symmetry (which can always be done whether or not the adjustment is important) and (ii) to impose two boundary conditions, one on each side of the equator, linking the analytical solutions to a profile of m that is marginally stable to inertial and barotropic instabilities.

b. Shallow-water system

Tidal theory provides an intuitively appealing way to understand the equatorial confinement of zonal jets (Theiss 2004; Scott and Polvani 2007) in a model governed by the shallow-water equations. In the limit of small positive equivalent depth, the latitudinal structure functions become increasingly confined close to

the equator (Flattery 1967; Longuet-Higgins 1968). In this limit the equatorial β -plane approximation is useful (Matsuno 1966; other references). The latitudinal structure functions are Hermite polynomials of order n multiplied by a Gaussian envelope with an e -folding scale equal to the equatorial radius of deformation. The equatorial deformation radius is analogous to the more familiar Rossby deformation radius of the midlatitudes, but its derivation includes an additional power of latitude y owing to the latitudinal variation of f , the Coriolis parameter. As a result, the relation between latitudinal and vertical scales for equatorial tidal motions is such that

$$\epsilon\beta^2y_0^4 = 1, \quad (4.1)$$

where $\epsilon = m^2/N^2 = 1/gh$ is the Lamb's parameter (Boussinesq limit), m is the vertical wavenumber, and h is equivalent depth. The latitudinal-scale factor y_0 varies as the square root of vertical wavelength, or one-fourth power of equivalent depth. For fixed equivalent depth, the Gaussian envelope is constant and the meridional extent of eigenmodes increases with mode index n as the order of the Hermite polynomial increases. This comment applies to equatorially trapped inertia-gravity and Rossby waves alike. Equatorial confinement of eigenfunctions at large ϵ occurs in more general flows with latitudinal shear that admit divergent barotropic and inertial instabilities (Dunkerton 1990; Winter and Schmitz 1998).

To the extent that zonal jets are driven by eddy PV fluxes⁵ in accord with the Taylor identity *and* there is no significant compensation owing to an induced mean meridional circulation, the appropriate generalization of the analytical model is to introduce a slowly varying Gaussian envelope such that

$$U = U(\xi) = U(0) \exp(-\xi^2) \quad (4.2a)$$

$$\xi = y/y_0 \quad (4.2b)$$

using the y_0 given by (4.1). Based on our results obtained with the barotropic model, we anticipate two

changes associated with the representation of jets in the shallow-water system. First, the choice of p (the power of cosine latitude) in the Rhines scaling [Eq. (2.3)], which was shown to be a rather minor factor in the analysis, becomes irrelevant when modes are confined to the tropics, where β is essentially constant. The spacing of (prograde) westerly jets does not vary significantly in latitude and the (retrograde) easterly jets are equal and comparable in strength to the westerly jets. Second, because the outermost jets decay to zero long before reaching the pole, the numerical calculation becomes ill conditioned in the sense that the global angular momentum constraint cannot determine the extent of the PV staircase accurately, if applied at the end of the calculation to determine μ_p , as done in the global problem. Noting the accuracy of the Taylor series expansions, we suggest an alternative procedure; namely, to regard the entire system of equations as a matrix problem for μ_j^2 and μ_p , constrained by (i) the shallow-water envelope for jet strength, (ii) jet spacing that is essentially constant, and (iii) the global conservation of absolute angular momentum. When truncated to two terms, the problem is almost linear in μ_j^2 save for a cubic term involving the outer contribution $\mu_p - \mu_N$. This term, however, may be included with the other linear terms when the assumption of constant spacing is made (specifically, to include the outermost step in the summation). We note incidentally that the matrix approach is also suitable for imperfect staircases designed with steps and risers of nonzero and finite slope, respectively.

It remains to be seen whether the shallow-water system is adequate for planetary atmospheres with vertical structure and overturning circulations (Plumb 1982) associated with thermal and mechanical forcings of the mean zonal flow. These circulations commonly act to offset eddy forcings so as to maintain gradient wind balance of the mean state. The net response (e.g., of U) to eddy forcing is therefore less than anticipated from eddy fluxes alone. More to the point, the induced mean meridional circulations vary in amplitude with latitude, introducing another variation in addition to that of (equatorially confined) eddy PV fluxes. It is thought that a PV staircase like that of Jupiter is less subject to the momentum-redistributing effects of radiative damping in the tropics than in midlatitudes (Scott and Polvani 2007) accounting for the pronounced tropical jets in comparison to those in midlatitudes (Ingersoll et al. 2004). This behavior was seen in one of Scott and Polvani's shallow-water experiments with radiative damping. A suitable analytical model of such a hybrid staircase requires, among other things, more detailed

⁵ The assumption of PV homogenization presumes an advective flux of PV substance, which, in effect, has the character of local or nonlocal diffusive mixing. This assumption is more reasonable for low-frequency Rossby waves that stir PV horizontally than for high-frequency inertia-gravity waves, which may overturn and break, leading to nonadvective fluxes of PV substance. Gravity waves may of course contribute to formation of PV jumps, as seen in the westerly phase of the quasi-biennial oscillation of the equatorial lower stratosphere. Additional knowledge of wave forcings is necessary to constrain the PV staircase, and the global angular momentum constraint must be extended to include the vertical dimension when the waves transport momentum vertically.

knowledge of the partial cancellation of eddy forcing and mean meridional circulation.

5. Conclusions

An idealized analytical model of the barotropic potential vorticity (PV) staircase was constructed with the guidance of recent numerical findings, constrained by global conservation of absolute angular momentum, perfect homogenization of PV in mixing zones between (prograde) westerly jets, and an imposed functional relationship between jet speed and their latitudinal separation using a multiple of the “dynamical Rossby wave” Rhines scale inferred from the strength of westerly jets. A barotropic model was employed here for (i) its simple relation between absolute angular momentum and PV (or absolute vorticity) and (ii) the model’s tendency (at large deformation radius) to produce westerly jets of approximately equal magnitude in a staircase extending to polar latitudes. Modes of arbitrary index were constructed assuming symmetry between hemispheres. Asymptotic analysis of the theoretical solution indicates a limiting ratio of jet spacing to dynamical Rhines scale equal to the square root of 6. In other words, westerly jets are spaced farther apart than predicted by the dynamical Rhines scale in order to satisfy the global angular momentum constraint and to maintain a barotropically stable configuration of the staircase.

We infer that an alternative *geometrical* Rhines scale for jet spacing can be obtained from conservation of absolute angular momentum on the sphere if the strength of zonal jets is known from other considerations. The geometrical argument complements the notion of a *dynamical* Rhines scale derived from the Rossby wave dispersion relation (Rhines 1975) and a *spectral* Rhines scale derived from the spectral flux of energy (Maltrud and Vallis 1991). Unlike the former, the geometrical Rhines scale is independent of the details of wave transport, PV mixing, and turbulence phenomenology. We merely require a PV staircase that (i) is completely homogenized within mixing zones located between (prograde) westerly jets and (ii) is barotropically stable. The evolution of the PV staircase originating from an upscale cascade of energy in the barotropic model is therefore seen to depend on conservation of energy (for the strength of jets) and conservation of absolute angular momentum (for the spacing and number of jets).

The numerical results suggest that an upscale energy cascade triggered by small-scale forcing leads to westerly jets and PV jumps that increase in amplitude with time but also occasionally merge, increasing the spacing

of, while decreasing the number of, jets and jumps. In a system where energy increases linearly in time owing to a constant injection of energy at small scales, the length of time between successive mergers varies roughly as the one-fourth power of time. Although individual mergers are always abrupt, the frequency of jet merger is low, and increasingly so with time, in these simulations. Closer examination of jet merger events suggests that the nearby flow approaches neutral stability prior to merger; that is, the PV step becomes nearly flat between adjacent jets. This result indicates that the temporal development of the staircase can be understood, to some extent, via the angular momentum constraint. Moreover, the geometrical Rhines scale provides a simple interpretation of the simulated variations of jet strength and spacing over a wide range of energy injection rates.⁶

We caution that the ideal PV staircase is a limiting, marginally stable profile; it does not describe observed staircases that are stable (having steps and risers of nonzero and finite slope, respectively) or unstable (having a sawtooth shape). It remains to be seen how well the angular momentum constraint governs the evolution and maintenance of *imperfect staircases*, the kind that one might encounter in a haunted house or on a mountain trail. As already noted, a simple modification of the ideal structure together with an alternative matrix method allows a similar analytic solution when the Taylor series are truncated to two terms. The question is not how to solve the problem, but how to constrain the modified staircase. It is reasonable to suppose that an observed staircase might appear subcritical to barotropic instability because the barotropic adjustment acts locally, not on the zonal mean. If external forcings are slow with respect to the adjustment, the mean zonal flow will remain stable by a finite amount. A statistical model taking into account the fraction of longitudes populated by barotropic instabilities should be sufficient to constrain a modified zonal-mean structure. This argument leaves unexplained the occurrence of apparently unstable staircases. For small supercriticality, a weakly nonlinear theory of the instability and its effect on the mean flow may be sufficient to constrain the PV staircase in a time-averaged sense.

⁶ We may imagine all such simulations concatenated into a single long simulation with an abrupt increase of injection rate between runs. In this case, jet mergers become increasingly separated in time. As an alternative, it would be interesting to perform a single experiment with an accelerating rate of injection (varying as t^4 , say) that would presumably trigger a series of mergers over a wide range n (decreasing from very large to small values) with roughly constant temporal spacing between merger events.

The concept of the PV staircase is evidently relevant to atmospheres with vertical structure other than equivalent barotropic in which radial exchanges of angular momentum may be important to the staircase structure. Application of our results to such systems is possible but the degree of difficulty depends on the nature of the vertical transport and whether it reinforces or overwhelms the processes responsible for staircase formation. Our analysis pertains to a simple flow system. The theoretical model and parameter choices were guided, in large measure, by the companion paper of Scott and Polvani, in the barotropic limit of the shallow-water system. Their setup is a forced configuration (random small-scale forcing), but one which also conserves angular momentum. The latter point was verified by close inspection of the numerical results. This forcing configuration—and others having the same property of zero net vertical transport of angular momentum—lies within the scope of the theoretical analysis of this paper.⁷ For a PV staircases (in other words, “jets”; Baldwin et al. 2007) to exist in more complex flows, the most important requirement is that the flow be vertically stratified, that is, that a *potential* vorticity (defined in terms of the vertical gradient of stratification) is meaningful and governs the evolution of the large-scale flow in all essential respects, namely, Rossby wave transport, forced overturning circulations, hydrodynamic instability, and quasi-2D turbulent lateral mixing. Absolute angular momentum is also relevant in such a system, but unlike PV, which, in substance form, is conserved between stratification isosurfaces (Haynes and McIntyre 1987), angular momentum may be transported vertically owing to stresses on the (vertically displaced) stratification isosurfaces.

In general, angular momentum of the entire body (atmosphere and whatever lies beneath) is conserved if the interaction with neighboring bodies is negligible. The concern, however, is not with the vertically averaged system, but with individual layers in which staircases may form. A shallow atmosphere atop another fluid layer or solid core may not, by itself, conserve angular momentum owing to radial exchanges of angular momentum. Three situations can be imagined. (i) If the underlying layer is a fluid (gas or liquid), presum-

ably this layer also supports waves and turbulence, so that one needs to consider the PV staircase as part of a multilayer system, connected by vertical wave propagation, mean meridional circulations, and turbulent stresses. In a balanced large-scale flow, forced overturning circulations (required to maintain balance) are coupled to PV transport and therefore have a coherent relationship to the staircase and its morphology. In cases of strong external forcing (e.g., tropical cyclone) the overturning circulation is relevant to staircase formation at leading order (and in extreme cases may be entirely responsible for the staircase). (ii) If the system consists of plasma, one may also need to consider electromagnetic forces that effectively exchange angular momentum within and between layers. (iii) If the underlying layer is a rigid solid core, exchanges of angular momentum between the surface and atmosphere simply alter the rotation rate of the core (length of day).

The last example reminds us that in the atmosphere above, any change in the meridional profile of axial angular momentum can be represented as the sum of a global mean (effective rotation rate) and departure therefrom. Because angular momentum is conserved in the entire system, global-mean changes of the solid and atmospheric angular momentum are exactly equal and opposite. In the atmosphere, the change of effective rotation rate expands or contracts the resting parabola, altering the slope of the resting PV profile. This alteration satisfies the integral conservation of PV substance, as the change in one hemisphere trivially cancels that in the other. If the same change of global mean were imposed on a preexisting ideal staircase, the perfect flatness of existing steps would be altered, subsequently requiring horizontal exchanges of angular momentum and PV in order to return to a perfect staircase. If these exchanges were local, that is, without transport across preexisting jets, the location and magnitude of jets would be altered in a predictable way, without knowing any details of the exchange other than that they are local. So, although we do not need to consider alterations of global-mean angular momentum in the Scott and Polvani system, we anticipate that the PV staircase thinking developed for our ideal case may be useful in a more general flow system in which some exchange of global-mean angular momentum with an underlying fluid or solid takes place. We also anticipate that it will be useful to decompose the problem into a global-mean contribution and staircase adjustment. The key point is that even when the details of horizontal and/or vertical exchange are not known, the PV staircase concept provides important guidance on realizable flow structures when the strength or spacing of jets is known from other considerations. The require-

⁷ The possibly important effect of cumulus momentum transport in the troposphere of Earth, and vertical transport in other deep convecting atmospheres, does not automatically preclude PV staircase thinking. Such forcings must be evaluated individually to ascertain whether systematic transport is occurring that might alter the staircase structure. Cumulus transports vary greatly according to, for example, how vertical wind shear organizes the convection (LeMone et al. 1998).

ment of hydrodynamic stability, in particular, applies to realizable staircases whether or not the global integral of angular momentum is conserved between any pair of stratification isosurfaces.

Acknowledgments. We thank Peter Rhines for his encouragement and for providing references to the literature on density staircases. This research was supported by National Science Foundation Grants ATM-0227632, ATM-0132727, and ATM-0527385.

REFERENCES

- Baldwin, M. P., P. B. Rhines, H.-P. Huang, and M. E. McIntyre, 2007: The jet-stream conundrum. *Science*, **315**, 467–468.
- Butchart, N., and E. E. Remsburg, 1986: The area of the stratospheric polar vortex as a diagnostic for tracer transport on an isentropic surface. *J. Atmos. Sci.*, **43**, 1319–1339.
- Cho, J. Y.-K., and L. M. Polvani, 1996: The emergence of jets and vortices in freely-evolving shallow-water turbulence on a sphere. *Phys. Fluids*, **8**, 1531–1552.
- Danilov, S., and D. Gurarie, 2004: Scaling, spectra and zonal jets in beta-plane turbulence. *Phys. Fluids*, **16**, 2592–2603.
- Del Sole, T., 2001: A simple model for transient eddy momentum fluxes in the upper troposphere. *J. Atmos. Sci.*, **58**, 3019–3035.
- Dickinson, R. E., 1968: Planetary Rossby waves propagating vertically through weak westerly wind wave guides. *J. Atmos. Sci.*, **25**, 984–1002.
- Dritschel, D. G., and M. E. McIntyre, 2007: Multiple jets as PV staircases: The Phillips effect and the resilience of eddy-transport barriers. *J. Atmos. Sci.*, **65**, 855–874.
- Dunkerton, T. J., 1980: A Lagrangian mean theory of wave, mean-flow interaction with applications to nonacceleration and its breakdown. *Rev. Geophys. Space Phys.*, **18**, 387–400.
- , 1981: On the inertial stability of the equatorial middle atmosphere. *J. Atmos. Sci.*, **38**, 2354–2364.
- , 1989: Nonlinear Hadley circulation driven by asymmetric differential heating. *J. Atmos. Sci.*, **46**, 956–974.
- , 1990: Eigenfrequencies and horizontal structure of divergent barotropic instability originating in tropical latitudes. *J. Atmos. Sci.*, **47**, 1288–1301.
- , 1991a: LIMS (Limb Infrared Monitor of the Stratosphere) observation of traveling planetary waves and potential vorticity advection in the stratosphere and mesosphere. *J. Geophys. Res.*, **96** (D2), 2813–2834.
- , 1991b: Nonlinear propagation of zonal winds in an atmosphere with Newtonian cooling and equatorial wavelike driving. *J. Atmos. Sci.*, **48**, 236–263.
- , and D. P. Delisi, 1985: The subtropical mesospheric jet observed by the Nimbus 7 Limb Infrared Monitor of the Stratosphere. *J. Geophys. Res.*, **90**, 10 681–10 692.
- , and D. J. O’Sullivan, 1996: Mixing zone in the tropical stratosphere above 10 mb. *Geophys. Res. Lett.*, **23**, 2497–2500.
- Flattery, T. W., 1967: Hough functions. Ph.D. dissertation, University of Chicago, 168 pp.
- Galperin, B., S. Sukoriansky, and H.-P. Huang, 2001: Universal $N(-5)$ spectrum of zonal flows on giant planets. *Phys. Fluids*, **13**, 1545–1548.
- , H. Nakano, H.-P. Huang, and S. Sukoriansky, 2004: The ubiquitous zonal jets in the atmospheres of giant planets and Earth’s oceans. *Geophys. Res. Lett.*, **31**, L13303, doi:10.1029/2004GL019691.
- Haynes, P. H., and M. E. McIntyre, 1987: On the evolution of vorticity and potential vorticity in the presence of diabatic heating and frictional or other forces. *J. Atmos. Sci.*, **44**, 828–841.
- Held, I. M., and A. Y. Hou, 1980: Nonlinear axially symmetric circulations in a nearly inviscid atmosphere. *J. Atmos. Sci.*, **37**, 515–533.
- Hitchman, M. H., and C. B. Leovy, 1986: Evolution of the zonal mean state in the equatorial middle atmosphere during October 1978–May 1979. *J. Atmos. Sci.*, **43**, 3159–3176.
- Holford, J. M., and P. F. Linden, 1999: Turbulent mixing in a stratified fluid. *Dyn. Atmos. Oceans*, **30**, 173–198.
- Huang, H.-P., and W. A. Robinson, 1998: Two-dimensional turbulence and persistent zonal jets in a global barotropic model. *J. Atmos. Sci.*, **55**, 611–632.
- , B. Galperin, and S. Semion, 2001: Anisotropic spectra in two-dimensional turbulence on the surface of a rotating sphere. *Phys. Fluids*, **13**, 225–240.
- Ingersoll, A. P., and Coauthors, 2004: Dynamics of Jupiter’s atmosphere. *Jupiter: The Planet, Satellites, and Magnetosphere*, Cambridge University Press, 105–128.
- James, I. N., and L. J. Gray, 1986: Concerning the effect of surface drag on the circulation of a baroclinic planetary atmosphere. *Quart. J. Roy. Meteor. Soc.*, **112**, 1231–1250.
- Kitamura, Y., and K. Ishioka, 2007: Equatorial jets in decaying shallow-water turbulence on a rotating sphere. *J. Atmos. Sci.*, **64**, 3340–3353.
- Lee, S., 2005: Baroclinic multiple zonal jets on the sphere. *J. Atmos. Sci.*, **62**, 2484–2498.
- LeMone, M. A., E. J. Zipser, and S. B. Trier, 1998: The role of environmental shear and thermodynamic conditions in determining the structure and evolution of mesoscale convective systems during TOGA COARE. *J. Atmos. Sci.*, **55**, 3493–3518.
- Lindzen, R. S., and A. Y. Hou, 1988: Hadley circulations for zonally averaged heating centered off the equator. *J. Atmos. Sci.*, **45**, 2416–2427.
- Longuet-Higgins, M. S., 1968: The eigenfunctions of Laplace’s tidal equations over a sphere. *Philos. Trans. Roy. Soc. London*, **262**, 511–607.
- Maltrud, M. E., and G. K. Vallis, 1991: Energy spectra and coherent structures in forced two-dimensional and beta-plane turbulence. *J. Fluid Mech.*, **228**, 321–342.
- Matsuno, T., 1966: Quasi-geostrophic motions in the equatorial area. *J. Meteor. Soc. Japan*, **44**, 25–43.
- McIntyre, M. E., 1982: How well do we understand the dynamics of stratospheric warmings? *J. Meteor. Soc. Japan*, **60**, 37–65.
- , and T. N. Palmer, 1983: Breaking planetary waves in the stratosphere. *Nature*, **305**, 593–600.
- , and —, 1984: The ‘surf zone’ in the stratosphere. *J. Atmos. Terr. Phys.*, **46**, 825–849.
- Orsolini, Y. J., V. Limpasuvan, and C. B. Leovy, 1997: The tropical stratopause in the UKMO stratospheric analyses: Evidence for a 2-day wave and inertial circulations. *Quart. J. Roy. Meteor. Soc.*, **123**, 1707–1724.
- Peltier, W. R., and G. R. Stuhne, 2002: The upscale turbulent cascade: Shear layers, cyclones and gas giant bands. *Meteorology at the Millennium*, R. P. Pierce, Ed., Academic Press, 43–61.
- Plumb, R. A., 1982: Zonally symmetric Hough modes and meridional circulations in the middle atmosphere. *J. Atmos. Sci.*, **39**, 983–991.

- , and A. Y. Hou, 1992: The response of a zonally symmetric atmosphere to subtropical thermal forcing: Threshold behavior. *J. Atmos. Sci.*, **49**, 1790–1799.
- Randel, W. J., and I. M. Held, 1991: Phase speed spectra of transient eddy fluxes and critical layer absorption. *J. Atmos. Sci.*, **48**, 688–697.
- Rhines, P. B., 1975: Waves and turbulence on a β -plane. *J. Fluid Mech.*, **69**, 417–443.
- Ruddick, B. R., T. J. McDougall, and J. S. Turner, 1989: The formation of layers in a uniformly stirred density gradient. *Deep-Sea Res.*, **36**, 597–609.
- Schneider, E. K., 1983: Martian great dust storms: Interpretive axially symmetric models. *Icarus*, **55**, 302–331.
- Scott, R. K., and L. M. Polvani, 2007: Forced-dissipative shallow-water turbulence on the sphere and the atmospheric circulation of the giant planets. *J. Atmos. Sci.*, **64**, 3158–3176.
- , D. G. Dritschel, L. M. Polvani, and D. W. Waugh, 2004: Enhancement of Rossby wave breaking by steep potential vorticity gradients in the winter stratosphere. *J. Atmos. Sci.*, **61**, 904–918.
- Simmons, A. J., 1974: Planetary-scale disturbances in the polar winter stratosphere. *Quart. J. Roy. Meteor. Soc.*, **100**, 76–108.
- Smith, K. S., 2004: A local model for planetary atmospheres forced by small-scale convection. *J. Atmos. Sci.*, **61**, 1420–1433.
- Stull, R. B., 1984: Transient turbulence theory. Part I: The concept of eddy-mixing across finite distances. *J. Atmos. Sci.*, **41**, 3351–3367.
- Theiss, J., 2004: Equatorward energy cascade, critical latitude, and the predominance of cyclonic vortices in geostrophic turbulence. *J. Phys. Oceanogr.*, **34**, 1663–1678.
- Tung, K. K., and J. S. Kinnery, 2001: Mechanisms by which extratropical wave forcing in the winter stratosphere induces upwelling in the summer hemisphere. *J. Geophys. Res.*, **106**, 22 781–22 791.
- Vallis, G. K., and M. E. Maltrud, 1993: Generation of mean flows and jets on a beta plane and over topography. *J. Phys. Oceanogr.*, **23**, 1346–1362.
- Williams, G. P., 1978: Planetary circulations: 1. Barotropic representation of Jovian and terrestrial turbulence. *J. Atmos. Sci.*, **35**, 1399–1426.
- Winter, Th., and G. Schmitz, 1998: On divergent barotropic and inertial instability in zonal-mean flow profiles. *J. Atmos. Sci.*, **55**, 758–776.
- Yoden, S., and M. Yamada, 1993: A numerical experiment on two-dimensional decaying turbulence on a rotating sphere. *J. Atmos. Sci.*, **50**, 631–643.